Tectonophysics 691 (2016) 65–84

Contents lists available at ScienceDirect

Tectonophysics

journal homepage: www.elsevier.com/locate/tecto

Geophysical analysis of the Alpha–Mendeleev ridge complex: Characterization of the High Arctic Large Igneous Province

G.N. Oakey [a,*], R.W. Saltus [b,1]

[a] Geological Survey of Canada (Atlantic), PO 1006, B2Y 4A2 Dartmouth, NS, Canada
[b] US Geological Survey, Mail Stop 964, Box 25046, Denver, CO 80225-0046, USA

ARTICLE INFO

Article history:
Received 6 July 2015
Received in revised form 30 June 2016
Accepted 8 August 2016
Available online 11 August 2016

Keywords:
Alpha Ridge
Mendeleev Ridge
High Arctic Large Igneous Province
Magnetic domain

ABSTRACT

The Alpha–Mendeleev ridge complex is a first-order physiographic and geological feature of the Arctic Amerasia Basin. High amplitude "chaotic" magnetic anomalies (the High Arctic Magnetic High Domain or HAMH) are associated with the complex and extend beyond the bathymetric high beneath the sediment cover of the adjacent Canada and Makarov–Podvodnikov basins. Residual marine Bouguer gravity anomalies over the ridge complex have low amplitudes implying that the structure has minimal lateral density variability. A closed pseudogravity (magnetic potential) contour around the ridge complex quantifies the aerial extent of the HAMH at ~1.3×10^6 km^2.

We present 2D gravity/magnetic models for transects across the Alpha Ridge portion of the complex constrained with recently acquired seismic reflection and refraction data. The crustal structure is modeled with a simple three-layer geometry. Large induced and remanent magnetization components were required to fit the observed magnetic anomalies. Density values for the models were based on available seismic refraction P-wave velocities. The 3000 kg/m^3 lower crustal layer is interpreted as a composite of the original crustal protolith and deep (ultramafic) plutonic intrusions related to a plume sourced (High Arctic) LIP. The 2900 kg/m^3 mid-crustal and 2600 kg/m^3 upper-crustal layers are interpreted as the combined effect of sills, dikes, and flows. Volumetric estimates of the volcanic composition include (at least) 6×10^6 km^3 for the mid- and upper-crust and between 13×10^6 and 17×10^6 km^3 within the lower crust — for a total of ~20×10^6 km^3.

We compare the magnetic structure, pseudogravity, and volumetric estimates for the HAMH portion of the HALIP with global large igneous province analogs and discuss implications for Arctic tectonics. Our results show that the closest analog to the HAMH/HALIP is the Kerguelen Plateau, which is considered a continental plateau intensively modified by plume-related volcanism.

1. Introduction

1.1. Arctic Amerasia Basin physiography

The study area for this paper encompasses much of the Amerasia Basin surrounding the Alpha and Mendeleev ridges (Fig. 1). The Alpha and Mendeleev ridges are the eastern (Alpha) and western (Mendeleev) components of a continuous seafloor high (bathymetric elevations range from approximately 3500 mbsl to 2500 mbsl) that extends from the Ellesmere Island portion of the Canadian Polar Margin (eastern side) to the East Siberian Shelf (western side; see Fig. 1). The overall high is approximately 2000 km long and 200–400 km wide. For submarine elevations shallower than 2500 mbsl, the Alpha and Mendeleev ridges are two separately labeled oceanic features divided at a saddle (approximate depth 2700 mbsl) known as Cooperation Gap (Treshnikov et al., 1966). The shallowest portions of both the Alpha and Mendeleev ridges are above 1000 mbsl.

The Lomonosov Ridge is a long (~1600 km) and narrow (typical width about 170 km) seafloor high (reaches submarine elevations above 1000 mbsl) separating the Eurasia Basin from the Amerasia Basin. The Lomonosov Ridge is a sliver of high standing continental crust that was separated from the Barents shelf as a result of Cenozoic seafloor spreading in the Eurasia Basin.

Between the Alpha–Mendeleev ridge complex and the Lomonosov Ridge lie the Makarov and Podvodnikov basins with seafloor depths >3500 mbsl. The Chukchi Borderlands is a bathymetrically complex, high-standing seafloor feature situated between the Alpha–Mendeleev ridge complex and the Bering Sea Shelf. The Canada Basin is a large deep water region (depths >3500 mbsl) bordered by the Alpha–

* Corresponding author.
E-mail address: Gordon.Oakey@Canada.ca (G.N. Oakey).
[1] Now at University of Colorado, Cooperative Institute for Research in Environmental Sciences, NOAA National Centers for Environmental Information, Boulder, CO 80305-3328, USA.

http://dx.doi.org/10.1016/j.tecto.2016.08.005

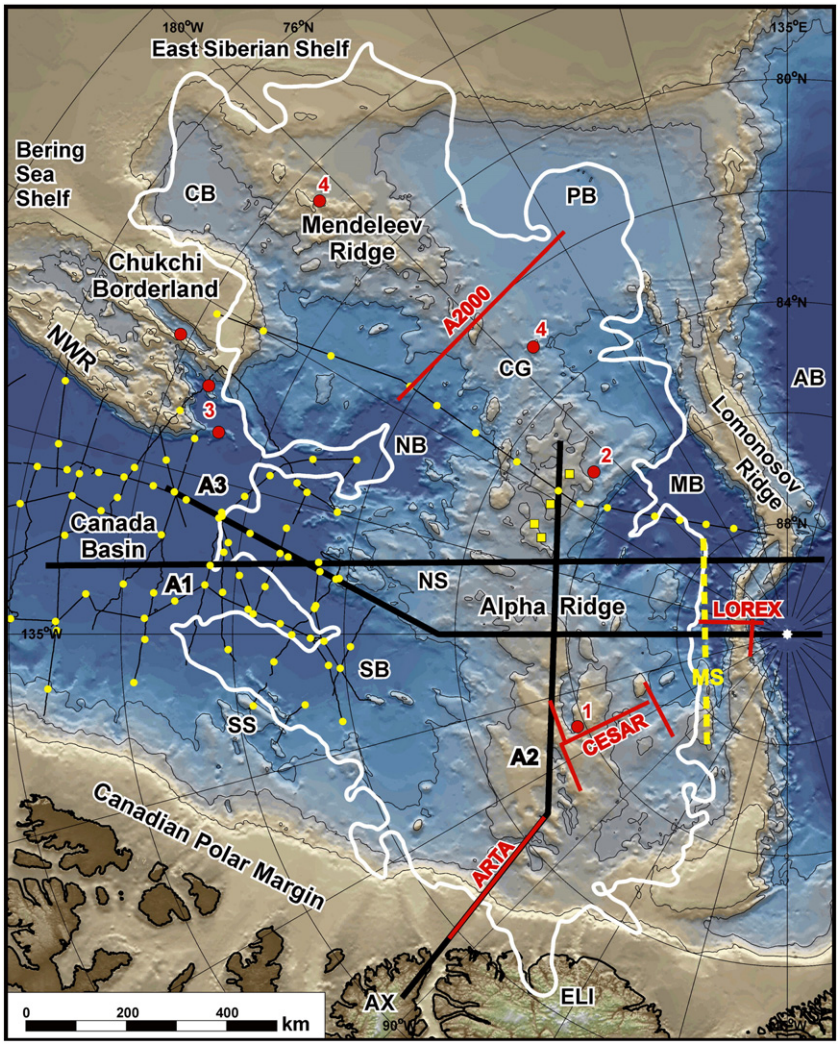

Fig. 1. Bathymetry/topography of the study area. International Bathymetric Chart of the Arctic Ocean (IBCAO; Jakobsson et al., 2012). The outline of the High Arctic Magnetic High (HAMH, white polygon) is from Fig. 3. Heavy black lines (labeled A1, A2, and A3) show the locations of the geophysical models. Solid red lines show the locations of published transects across the Alpha and Mendeleev ridges discussed in the text: A2000 from Lebedeva-Ivanova et al. (2006); ARTA from Funck et al. (2011); CESAR from Forsyth et al. (1986a,b); LOREX from Forsyth and Mair (1984). Thin black lines show locations of (2007 to 2011) Louis S St. Laurent seismic reflection data. Yellow dots show locations of (2007 to 2011) sonobuoy deployments (Chian and Lebedeva-Ivanova, 2015). Yellow squares show sonobuoy locations from Jokat et al. (2013). Red dots show locations of volcanic samples: 1) Van Wagoner et al. (1986); 2) Jokat et al. (2013); 3) Brumley et al. (2013); Mukasa et al. (2009, 2015); 4) Morozov et al. (2013 a,b). The axis of Marvin Spur (MS) is shown with a yellow dotted line. AB = Amundsen Basin; AX = Axel Heiberg Island; CB = Chukchi Basin; CG = Cooperation Gap; ELI = Ellesmere Island; NB = Nautilus Basin; NS = Nautilus Spur; NWR = Northwind Ridge; MB = Makarov Basin; PB = Podvodnikov Basin; SB = Stefansson Basin; SS = Sever Spur.

Mendeleev ridge complex, the Canadian Polar Margin, the Chukchi Borderlands, and the Alaskan Polar Margin.

1.2. Early geophysical interpretations for the High Arctic

The earliest regional Arctic magnetic interpretations were published in the 1960s and early 1970s based on reconnaissance profiles collected at very high altitude (20,000 ft) in the early 1950s by the U.S. Air Force and Coast and Geodetic Survey and in the 1960s at low altitude (450 m) by the University of Wisconsin (Ostenso, 1962; King et al., 1964, 1966; Ostenso and Wold, 1971). US Geological Survey researchers King et al. (1964, 1966) identified and mapped a "Central Magnetic Zone" that with "considerable confidence" they interpreted (based on comparison with magnetic profiles from the Canadian Shield) as a "large sunken block of continental rocks".

Ostenso and Wold (1971), in contrast, working with the same set of magnetic profiles, concluded that the profiles crossing the Alpha Ridge were consistent with similar profiles across the Atlantic Ridge near Iceland. Vogt and Ostenso (1980) modeled gravity profiles from floating ice islands T-2 and T-3 along with the early magnetic profiles to further pursue an Atlantic Ridge analog interpretation for the "Alpha Cordillera" (their terminology). The U.S. Navy collected a series of magnetic profiles across the central Alpha Ridge and much of the Canada Basin in 1977 and 1978. Taylor et al. (1981) analyzed these profiles over the Alpha Ridge and concluded (1) the Alpha Ridge magnetic character continued beneath the sedimentary cover of Canada Basin, (2) the high amplitude magnetic anomalies of the Alpha Ridge were not consistent with sea floor spreading parallel to the ridge axis, and (3) the high amplitude and irregular Alpha Ridge anomalies are similar to magnetic patterns observed near Iceland.

Operating from more recent magnetic and gravity data grids, numerous authors have associated the large amplitude magnetic patterns in the Alpha–Mendeleev region with large volumes of basaltic rock (e.g., Piskarev, 2004; Lebedeva-Ivanova et al., 2006; Vogt et al., 2006; Grantz et al., 2009, 2011; Døssing et al., 2013). Based on "back of the envelope" magnetic and isostatic arguments, Vogt et al. (2006) gave an estimate of 10×10^6 km^3 mafic volume for the Alpha–Mendeleev volcanic province. Using an unpublished magnetic data compilation, Grantz et al.

(2009) mapped boundaries of a magnetically defined "Alpha–Mendeleev LIP". Saltus et al. (2011) used the IPY (International Polar Year) magnetic compilation (Gaina et al., 2011) to define circum-Arctic magnetic domains and included a (slightly) revised version of the Grantz et al. (2009) "Alpha–Mendeleev LIP" Domain. Døssing et al. (2013) examined, in some detail, the magnetic expression of the Alpha Ridge portion of the High Arctic Magnetic High Domain (HAMH), and concluded that it represents a portion of the High Arctic Large Igneous Province (HALIP), and further suggested that it represents the core source region for the HALIP.

Gaina et al. (2014) provided a comprehensive review of geophysical data (including regional gravity, magnetics, and seismic tomography) for the circum-Arctic and summarized the many open tectonic questions for the region. They concluded that the "nature of both the Alpha and Mendeleev ridges remains speculative because extensive volcanism has overprinted and complicated the original geophysical signatures".

1.3. Velocity structure of the Alpha–Mendeleev ridge complex

Only three long-offset seismic refraction experiments have been carried out over the Alpha–Mendeleev ridge complex.

During the 1983 CESAR ice-camp operations (Jackson et al., 1985) four reversed refraction lines were acquired over central Alpha Ridge and the flank of Makarov Basin. The resulting velocity structures (Forsyth et al., 1986a,b; Asudeh et al., 1988) show a thin (~0.4 km) low-velocity (1.8 to 2.4 km/s) sedimentary succession overlying a "surprisingly uniform" upper crustal layer (Vp of 5.0–5.2 km/s), increasing to 6.5 km/s at depths of only ~8 km. Mid-crustal velocities continue to increase relatively smoothly, reaching values of Vp ~7.0 km/s at a maximum depth of ~24 km. They also document an anomalous low-velocity (6.8 km/s) mid-crustal block on their "strike" line to explain a time lag in the observed first arrivals. A high velocity lower crustal layer (Vp ~7.3 to 7.5 km/s) is documented on two their lines. Highly variable Moho depths (based on Vp velocities exceeding 8.0 km/s) ranged from 24 to 40 km beneath the central Alpha Ridge and 21–25 km beneath the flank of Makarov Basin. The deepest Moho depths correspond with the presence of the high velocity lower crust. These authors concluded that the Alpha Ridge is an Icelandic-type structure generated by mantle plume volcanism within an oceanic rift system.

The Arctic-2000 wide-angle refraction profile across central Mendeleev Ridge (Lebedeva-Ivanova et al., 2006) documents a significantly thicker sedimentary succession than the CESAR results. The uppermost (0.1 to 0.7 km thick) (pelagic?) layer-1 has a Vp of 1.7 km/s and overlies two higher velocity semi-consolidated and lithified siliciclastic layers. Vp for layer-2 range from 2.3 to 2.6 km/s and increase in thickness (max. 1.7 km) away from the ridge axis. Vp for layer-3 range from 3.2 to 3.6 km/s with maximum thicknesses of 1.2 to 1.6 km on the "arch of the Mendeleev Ridge" and "western flank" (towards Podvodnikov Basin) and a minimum thickness (0.2 to 0.3 km) on the "eastern slope". It is unclear whether the thicker sedimentary succession documented over the Mendeleev Ridge (> 3.0 km) when compared with the CESAR results over Alpha Ridge (< 0.5 km) is an indication of different (older?) sedimentary processes, or simply a limitation of the resolution of the CESAR refraction data. The crustal structure of the Arctic-2000 line shows a 3.6 to 4.0 km thick upper crustal layer (Vp of 5.0 to 5.4 km/s) overlying a mid-crustal layer (Vp of 5.9–6.5 km/s) with a maximum thickness of 4 km. The lower crust (Vp of 6.7 to 7.3 km/s) is between 19 and 21 km beneath the central Mendeleev Ridge arch, and thins to <10 km beneath the flanks. A continuous high velocity layer (Vp of 7.4 to 7.8 km/s) is ~7 km thick beneath the arch and thins to either side (~5 km thick to the east and ~3 km to the west). Lebedeva-Ivanova et al. (2006) interpreted this layer as a crust–mantle 'mixed layer', perhaps the result of underplating. Moho (Vp of 7.9 to 8.0 km/s) reached a maximum depth beneath the central arch. These authors concluded that the Mendeleev Ridge was "composed of continental [crust] that has been substantially altered during the development of the deep Arctic Basin and associated magmatism".

The ARTA transect (Funck et al., 2011) extends from the coast of the Canadian Polar margin onto the axis of the Alpha Ridge. The continental margin is characterized by Vp values ranging from 5.5 to 6.6 km/s with Moho depths (Vp > 8.0 km/s) of ~30 km that thins abruptly to a depth of ~24 km. The margin is overlain by 2 to 6 km (Paleozoic? and younger) sedimentary successions (Vp of 3.0 to 4.6 km/s). A thin (~1 km) drape of low velocity sediments (Vp of 2.2 km/s) extends from the shelf onto Alpha Ridge. The velocity structure of Alpha Ridge crust is subdivided into three distinct layers. The upper (volcanoclastic) crust (Vp of 4.7 to 5.4 km/s) ranges from 3 to 5 km in thickness. The mid-crust (Vp of 6.1 to 6.6 km/s) ranges from 4 to 8 km in thickness. The lower-crust (Vp of 6.8 to 7.3 km/s) ranges from 20 to 24 km in thickness. Unlike the Mendeleev Ridge, a 6 to 8 km thick high-velocity (Vp of 7.5 to 7.6 km/s) "underplated" layer is only identified within the "transition zone" between the continental crust and the Alpha Ridge crust. Moho depths range from 26 to 32 km beneath the Alpha Ridge. These authors concluded that the Alpha Ridge was a volcanic plateau resulting from the "interaction between a plume and a seafloor spreading center".

Several authors have presented velocity structures over the Alpha–Mendeleev ridge complex from sonobuoy deployments (e.g. Jokat et al., 2013; Chian and Lebedeva-Ivanova, 2015). Although these data are extremely useful in establishing the regional continuity of the velocity structures, the short offsets (typically <35 km) are only able to resolve the sedimentary succession and uppermost crustal layers.

2. The High Arctic Large Igneous Province (HALIP)

A Large Igneous Province (LIP) is defined as a region where a large volume of (generally mafic) magma was generated and emplaced (e.g., Coffin and Eldholm, 1994; Bryan and Ernst, 2008; Ernst and Bleeker, 2010). Although there are examples where LIPs interact with sea-floor spreading or subduction processes (e.g., Meyer et al., 2007; Camp and Hanan, 2008), LIPs are considered to result from some other process, frequently attributed to the actions of a hotspot or mantle plume (Sleep, 1990, 1992; Coffin and Eldholm, 1994; Ernst and Buchan, 2001; Campbell, 2005; Ernst and Bleeker, 2010). In addition to the surface manifestation of regions with extensive basaltic rock present, LIPs include deeper magmatic plumbing systems including dike swarms, sills, layered intrusions, and deep mafic underplating. The term LIP was not widely used prior to about 1990, but documentation of large volume "hotspot" volcanism dates back to the 1970s. Well known global LIP examples include the Deccan Traps, Iceland, the Siberian Traps, Ontong Java Plateau, Kerguelen, and the Columbia River Basalts (e.g., Coffin and Eldholm, 1994; Ernst and Bleeker, 2010).

The presence and tectonic importance of inferred hotspot activity in the high arctic was introduced and discussed from the late 1970s to the mid 1990s by a number of authors (e.g., Vogt et al., 1979; Weigand and Testa, 1982; Worsley, 1986; Weber, 1990; Lawver and Mueller, 1994). To our knowledge, Tarduno (1998) and Maher (2001) were the first to apply the term High Arctic Large Igneous Province (HALIP) to a broad portion of the high Arctic, including the Alpha Ridge and portions of Svalbard and northern Canada. Despite these and many more publications relating or referring to the HALIP, this LIP is not uniformly recognized nor included in all tectonic models of the Amerasia Basin (e.g., see reviews by Lawver and Scotese, 1990, and Miller et al., 2010). Gaina et al. (2014) examined the HALIP relative to the paleo-position of the Iceland plume and concluded that the Iceland plume is an unlikely source for the HALIP. They did conclude however that the HALIP was formed, at least in part, above a mantle "plume generation zone" (Torsvik et al., 2006) that provided a possible source.

2.1. HALIP rock samples from the Canadian and Eurasian margins

Maher (2001) provides a general summary of sample age ranges and geochemical character for Cretaceous magmatic rocks from various HALIP localities including Franz Josef Land, Svalbard, Northern

Greenland, and the Canadian Arctic. The composite age span for these combined localities spans from 140 to 90 Ma with a possible 70 Ma age cited for Northern Greenland and late stage volcanism as late as 65 Ma on the Canadian margin. The Franz Josef, Svalbard, and Northern Greenland samples are from mafic and intermediate dikes, sills, and flows. The Canadian Arctic has the largest sampled region which

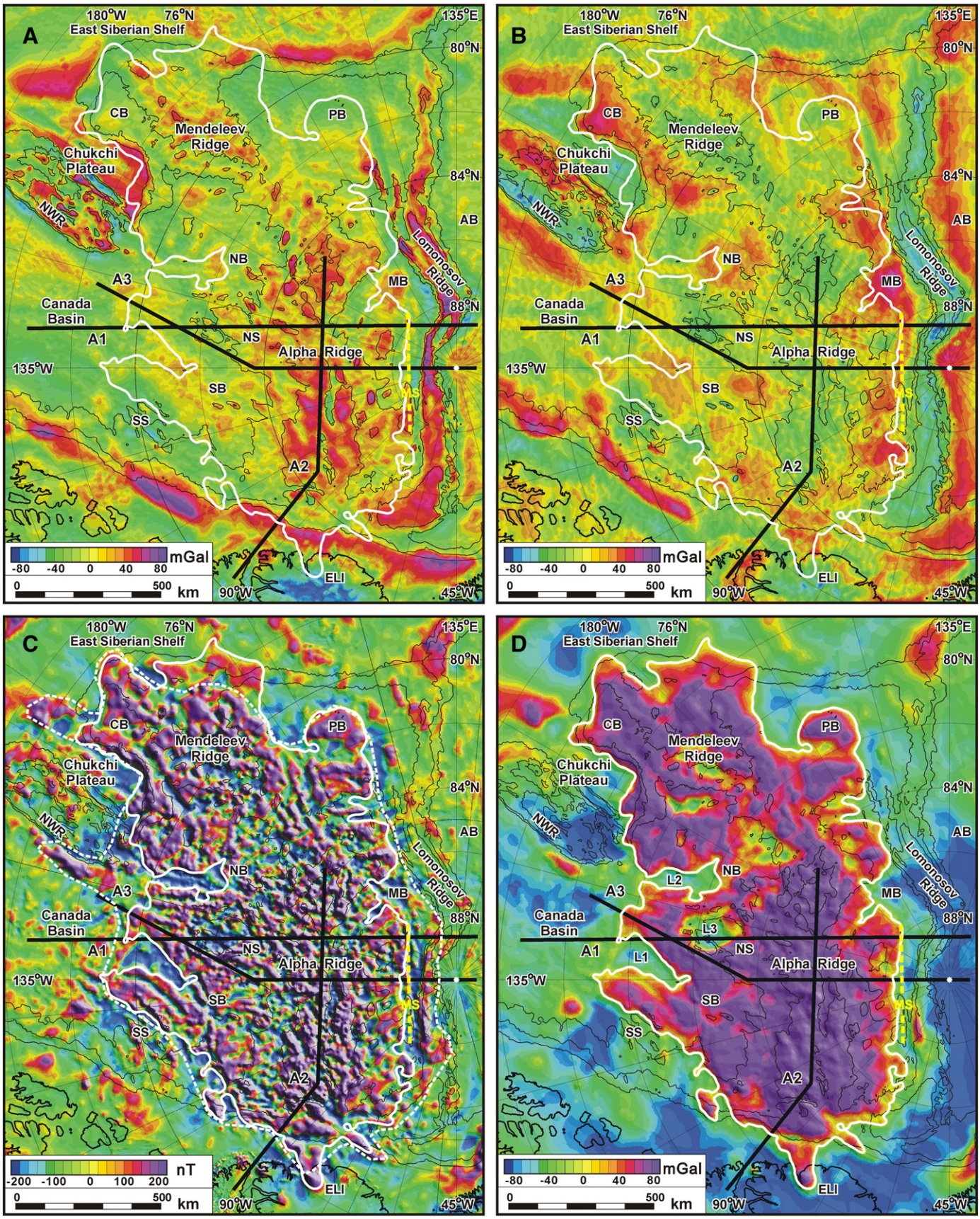

includes broadly distributed and voluminous flood basalts, sills, dikes, and plutons. Although ages of the volcanic rocks range from early Cretaceous to early Paleogene, three main pulses have been identified (Estrada et al., 2016): (1) 130 to 115 Ma regional basalt volcanism from the Axel Heiberg area (Embry and Osadetz, 1988) and Ellef Ringnes Island (Evenchick et al., 2015); (2) 102 to 95 Ma voluminous basalt flows of the Strand Fiord Formation on Axel Heiberg and surrounding islands (Ricketts et al., 1985; Embry and Osadetz, 1988; Embry, 1991; Estrada and Henjes-Kunst, 2013; Tarduno, 1998; Balkwill, 1983; Evenchick et al., 2015; Osadetz and Moore, 1988; Estrada, 2015). The first two pulses include associated mafic tholeiitic dikes and sills (e.g. Balkwill, 1978; Embry, 1991; Buchan and Ernst, 2006; Evenchick et al., 2015; Villeneuve and Williamson, 2006; Estrada and Henjes-Kunst, 2013). The NE–SW trends of these dikes suggest a possible mantle plume centre beneath the Canadian end of the Alpha Ridge (Embry and Osadetz, 1988; Buchan and Ernst, 2006; Døssing et al., 2013); (3) 93 to 65 Ma late-stage alkaline, mafic to felsic igneous suites (Estrada and Henjes-Kunst, 2004, 2013; Trettin and Parrish, 1987; Embry and Osadetz, 1988).

2.2. Offshore sampling of the HALIP

Relatively few rock samples have been collected from the Alpha–Mendeleev ridge complex itself, and of these, only a few published and reliable age dates are available (see locations in Fig. 1). The first samples from Alpha Ridge were from the 1983 CESAR ice camp operations (Jackson et al., 1985). These dredge samples were highly altered and age dating was not possible; however, the bulk geochemistry (Van Wagoner et al., 1986) clearly identified alkalic basalts which "strongly suggests that the Alpha Ridge was not formed by volcanism at an island arc or a mature spreading centre".

Morozov et al. (2013a,b) report U–Pb ages of 127 Ma for a drilled sample from the northern Mendeleev Ridge (near Cooperation Gap) and another on southern Mendeleev Ridge with a date of 260 Ma. Jokat et al. (2013) document an Ar–Ar age of 89 ± 1 Ma for a basalt sample (PS051-041-1cc) collected on central Alpha Ridge. Brumley (2014) and Mukasa et al. (2015) report Ar–Ar ages of 112 Ma, 100 Ma and 85–73 Ma for basaltic samples from the Mendeleev Ridge and Chukchi Borderland. These younger ages are in the same general range as the ages of HALIP-related igneous rocks from onshore areas of the Canadian Polar margin (Estrada et al., 2016).

The apparent long-lived nature (130 to 80 Ma) of igneous activity in the HALIP region is a topic of current discussion and debate (e.g. Mukasa et al., 2015). Current Arctic tectonic models (e.g. Shephard et al., 2013) include possible complex combinations of LIP and rifting/seafloor spreading as contributors to the origin of the Alpha–Mendeleev ridge complex. In their circum-Arctic review Gaina et al. (2014) characterize an early (130–80 Ma) tholeiitic phase (which they associate with a likely plume source) and a more recent (85–60 Ma) alkaline phase attributed to non-plume volcanism (Buchan and Ernst, 2006; Tegner et al., 2011).

In summary, basaltic material from high Arctic regions associated with the HALIP (Tarduno, 1998; Maher, 2001; Kingsberry et al., 2014) and from dredge samples of the Alpha and Mendeleev ridges (Andronikov et al., 2008; Mukasa et al., 2009, 2015; Brumley et al., 2013; Petrov et al., 2015) generally show two broad sets of ages, one ranging from about 130 to 120 Ma, and the other from 90 to 80 Ma. Overall the submarine (Alpha–Mendeleev) portion of the HALIP is poorly sampled.

3. Gravity and magnetic compilations of the Arctic

The gravity data used in this study are from the Andersen et al. (2010) global free air gravity compilation, which combined the Danish National Space Center's DNSC08GRA 1-arcminute global marine gravity (obtained from satellite altimetry) and the EGM2008 5-arcminute gravity anomalies on land (Pavlis et al., 2008). Gravity anomalies from the Kenyon et al. (2008) Arctic Geoid Model (ArcGP version 06-01) and laser altimetry from ICESat (Zwally et al., 2002) were used to close the polar gap in the satellite coverage.

The magnetic anomaly data used in his study is from the International Polar Year Circum-Arctic Mapping Project (CAMP) compilation (Gaina et al., 2011).

3.1. Marine free air gravity anomaly/onshore Bouguer gravity anomaly

Since the onshore free air gravity is dominated by topographic effects, both terrain and Bouguer corrections were applied using the elevation model obtained from the IBCAO Version 3.0 gridded data set (Jakobsson et al., 2012). The corrections were derived using a technique to calculate the cumulative effect of 3-D cubes (Nady, 1966; Oakey, 2005), each with an area of 500 × 500 m and 100 m thick using a crustal density of 2670 kg/m^3. Ice covered areas were further corrected using the Bamber et al. (2001a,b) ice thickness model for Greenland and the ice thickness model for Arctic Canada of Oakey and Stephenson (2008); the ice density was specified as 900 kg/m^3. Since the topography in the IBCAO compilation has a significantly higher resolution than the gridded gravity data, the calculated (full-resolution) Bouguer correction has a higher frequency content. Pre-filtering (or re-gridding) of the topography significantly reduces the dynamic range of the elevation values and does not adequately compensate the topographic effects. It was determined that the optimal solution was to compute the full-resolution Bouguer correction and then apply a 24 km low-pass filter (which is slightly larger than the Nyquist frequency of the 5 arc-minute gravity grid) prior to adding to the free air gravity.

Free air gravity anomalies over the Alpha–Mendeleev Ridge (Fig. 2A) show an irregular pattern of positive and negative anomalies (±60 mGal) which generally correspond with bathymetric highs and lows. Large free air gravity highs (>80 mGal) are associated with the Lomonosov Ridge and bathymetric highs over the Chukchi Plateau. Semi-continuous "shelf-edge" gravity highs (in places >100 mGal) extend along the entire length of the Canadian Polar Margin and segments of the East Siberian Shelf. Low amplitude (<−40 mGal) gravity lows extend over most of Canada Basin; however, there is a broad gravity high (~20 mGal) adjacent to Northwind Ridge. Most of Stefansson Basin exhibits positive free-air anomalies (>20 mGal) and there are numerous isolated highs and lows over Nautilus Basin. The Makarov and Podvodnikov basins generally have a negative free air gravity anomaly

Fig. 2. Potential field maps of the study area. The Andersen et al. (2010) global free air satellite-derived gravity compilation and the International Polar Year (IPY) CAMPM magnetic compilation (Gaina et al., 2011) were used in this study. Featured are the outline of the newly-defined HAMH domain boundary (thick white line); the locations of the three modeled transects (thick black lines) and the 1000 m bathymetric contours (thin black lines). Abbreviated place names are from Fig. 1. 2A) Marine free air/onshore Bouguer Gravity Anomalies. The onshore portion of the gravity field has been Bouguer corrected using a crustal density of 2670 kg/m^3 and 900 kg/m^3 for ice. 2B) Onshore/offshore Bouguer Gravity Anomalies. A marine Bouguer correction has been applied to remove effects of bathymetric relief. The water column was (numerically) replaced with crustal density rocks (2670 kg/m^3) using the bathymetry from the IBCAO Version 3.0 gridded data set. A 1000 km high-pass filter was applied to remove (long-wavelength) isostatic effects. 2C) Total-field magnetics. The magnetic anomalies over the Alpha–Mendeleev ridge complex show high amplitude "chaotic" patterns that extend beneath the sedimentary cover of the Canada Basin and the Makarov–Podvodnikov basins. The "F1 Alpha–Mendeleev LIP" magnetic domain (Saltus et al., 2011) (dashed white line) is shown to compare with our new HAMH domain boundary. 2D) Pseudogravity. Pseudogravity (aka magnetic potential) was calculated using a Fourier-domain inversion method which converts the magnetic dipole source to a monopole source. A magnetic field strength of 8.0 A/m was "replaced" mathematically with an equivalent density of 2670 kg/m^3. The closed contour (isoline) of the pseudogravity covers an area of ~1.3 × 10^6 km^2. The two deeply incised "notches" (L1 and L2) observed in the Canada Basin side of the HAMH isoline boundary correspond with large negative magnetic anomalies (see Fig. 2C) and may represent areas with reverse polarity remanent magnetization. L3 = pseudogravity low over Nautilus Spur.

(<−40 mGal), although a few locations with a positive anomaly are directly correlated with bathymetric features in these basins.

3.2. Marine Bouguer gravity anomaly

The medium and short wavelength free air gravity anomalies are dominated by effects caused by the bathymetric relief (i.e., positive gravity anomalies correlate with bathymetric highs and gravity lows correlate with bathymetric lows). In order to remove these bathymetric effects, a marine Bouguer gravity anomaly was calculated with the IBCAO Version 3.0 compilation using the same technique applied to the onshore free air gravity (described in Section 3.1); however, a shorter high-pass filter was applied (12 km rather than 24 km). The water column (density of 1030 kg/m^3) was substituted with crustal density rocks (density of 2670 kg/m^3). A 1000 km high-pass Fourier filter was applied to restore (long-wavelength) isostatic equilibrium.

In general, mid- and short-wavelength (<100 km) residual Bouguer gravity highs can be caused either by basement highs (buried beneath sedimentary cover and therefore not removed by the Bouguer correction) or high density crustal blocks (e.g., dense mafic intrusions in continental crust). The resulting residual marine Bouguer gravity anomalies (Fig. 2B) show a semi-continuous low (−40 to −30 mGal) over the Alpha–Mendeleev ridge complex with no significant variation, which implies that there is minimal lateral variability in the density structure (consistent with interpretations of Weber, 1986; Dove et al., 2010). Pronounced Bouguer gravity lows (<60 mGal) are associated with both the Lomonosov Ridge and the Northwind Ridge, which suggests that the structures include significant thicknesses of low-density (sedimentary?) material. The shelf-edge anomalies along the Canadian Polar Margin and East Siberian Shelf have been significantly reduced, and in some locations eliminated. Longer wavelength (>100 km) highs can also be produced over sedimentary basins that are not isostatically balanced (i.e. the sediment volume is replacing water rather than crust). The residual shelf-break Bouguer anomalies on the Canadian Polar Margin may represent either thick non-isostatically compensated sedimentary basins or deep high-density basement structures. The residual Bouguer gravity highs (>40 mGal) over the Chukchi, Makarov, Nautilus, and Stefansson basins are interpreted to be the result of non-isostatically compensated sedimentary basins.

3.3. Total field magnetic anomaly

The magnetic anomaly data (Fig. 2C) show a distinctive domain of high-amplitude magnetic highs and lows with a chaotic map pattern over the Amerasia Basin, classified by Saltus et al. (2011) as the "Alpha–Mendeleev LIP". Based on more detailed analysis, we have refined the boundaries of this domain which we call the HAMH. Within the HAMH magnetic anomaly values in the circum-Arctic (Gaina et al., 2011) grid range from −950 to +1370 nT. The original domain of Saltus et al. (2011) spans an area of 1.5×10^6 km^2 with an oblong shape that is roughly 1780 km on the long axis by 885 km on the shorter axis.

3.4. Pseudogravity (magnetic potential) — definition of the HAMH

To quantitatively define the boundaries and highlight the long-wavelength (and thus deeper) nature of the HAMH we use the pseudogravity transformation. Pseudogravity (also known as magnetic potential; see Blakely, 1995) is an alternate mathematical expression of total-field magnetic anomalies. This transformation is calculated in the Fourier frequency domain as a function of 1/r where r is the wavenumber. The transformation also includes an angular component based on magnetic inclination. The transformation to pseudogravity "simplifies" the resulting field (as compared to the original dipole total-field) in two fundamental ways: (1) the transformation removes the asymmetric dipole effects of geomagnetic latitude on the form of anomaly patterns, and (2) the transformation changes the depth-to-source dependence from distance cubed to distance squared. The transformed field has depth-to-source dependence characteristics similar to that of gravity data (thus the term "pseudogravity").

For regional scale geologic interpretation and modeling, pseudogravity provides a greater emphasis on deeper portions of the crust and on thicker physical property domains versus standard total-field magnetic anomalies. For example, the pseudogravity anomaly resulting from a spherical magnetic source body is a single discrete high centered above the source body. The total-field magnetic expression of the same source body is a combination of magnetic lows and highs in which the relative location and strength of the component highs and lows are dependent on the geomagnetic latitude — the anomaly pattern at high latitude is a central high surrounded by a circular low "moat" whereas the pattern at mid latitudes is skewed so that the low zone is asymmetric and the center of the high is shifted away from the source midpoint. For our study, the geomagnetic pole is within the area, so an average near 90° magnetic inclination value does not produce these "phase-component" artifacts.

As a practical matter, when converting from a total-field magnetic anomaly grid to pseudogravity, the resulting transformation will inevitably include a spurious long-wavelength tilt as a result of the incomplete representation of the longest wavelength total-field anomalies in the original grid (e.g., the ideal transformation would take place at the center of an infinite grid). We remove this spurious trend using a 2000 km high-pass filter. The resulting pseudogravity field is shown in Fig. 2D. The parameters used in calculating the pseudogravity are a "replacement" of a magnetic field strength of 8.0 A/m with a density equivalent of 2670 kg/m^3. Changing this ratio will affect the resulting pseudogravity amplitude ranges, but is only a linear scalar effect and does not impact the resulting geometry of the HAMH.

The pseudogravity representation allows for a robust, repeatable, and quantifiable mapping of the HAMH domain boundary following a pseudogravity isoline (a closed contour around the high values) as shown in Fig. 2D. We describe the geometry of the HAMH boundary in Section 4. In summary: we define the HAMH as a distinctive zone of high amplitude magnetic highs and lows with no single directional pattern that falls within a closed pseudogravity high. The aerial extent of the HAMH (~1.3×10^6 km^2) encompasses the Alpha–Mendeleev ridge complex as well as some of the adjoining deep water regions including portions adjacent to the Canada and Makarov–Podvodnikov basins.

4. Association of the HAMH with the HALIP

We interpret the HAMH as a geophysical manifestation of the voluminous mafic intrusions and extrusions of the HALIP in the region surrounding and including the Alpha–Mendeleev ridge complex. A primary reason for this conclusion is the spatial coincidence of the geophysical domain and the known and inferred extent of LIP igneous geology for the Alpha–Mendeleev ridge complex (e.g., Maher, 2001).

We are not the first to associate high-amplitude magnetic anomalies in the high Arctic with LIP volcanism. Weber (1986, 1990) concluded from examination and modeling of gravity and bathymetry from the 1983 "Canadian Expedition to Study the Alpha Ridge" (CESAR), available magnetic profiles, and satellite magnetic anomalies that the Alpha Ridge consists of a relatively homogeneous mafic crust, consistent with a plume (hotspot) origin source as suggested by Forsyth et al. (1986a,b). We agree with many of Weber's (1986, 1990) conclusions and, with the benefit of more comprehensive magnetic data coverage and additional geophysical constraints, can model the HAMH with greater detail and confidence. Gaina et al. (2014) cite an overprint of extensive volcanism as a characteristic of the Alpha–Mendeleev ridge complex. It is exactly this extensive component that we seek to characterize.

The "F1" (Alpha–Mendeleev Large Igneous Province — LIP) Domain described by Saltus et al. (2011) was based on a qualitative assessment of high amplitude magnetic anomalies over the Amerasia Basin. The F1 Domain (Fig. 2C) covers an area of ~1.5×10^6 km^2 and includes a significant portion of the Lomonosov Ridge, the shelf region of the Canadian Polar Margin, and the magnetic highs along the Canada Basin edge of the Chukchi Plateau (adjacent to Northwind Ridge, Figs. 1 and 2C). Our revised HAMH definition (Figs. 1 and 2) is based on a closed contour in the calculated magnetic potential (aka. pseudogravity), and represents the geographic area of the HALIP (~1.3×10^6 km^2) with a deep-crustal root. Using this definition, the Lomonosov Ridge is not included, and the new boundary lies (approximately) along the Marvin Spur (MS) (Figs. 1 and 2). The revised HAMH boundary shows that (in addition to the Canadian Polar Margin) the Domain extends to onshore Ellesmere Island. The pseudogravity-defined HAMH does not include the high amplitude magnetic anomalies adjacent to Northwind Ridge — indicating that the magnetic sources of these features do not a have a deep-crustal root. The new HAMH Domain now includes a portion of the East Siberian Shelf, which was not part of the Saltus et al. (2011) F1 Domain.

On the Canada Basin flank of the Alpha Ridge, the HAMH boundary has two pronounced embayments: one within Nautilus Basin; the other within Stefansson Basin. These correspond with large negative magnetic lows (L1 and L2). We speculate that these magnetic lows are over non-magnetic (continental?) crustal blocks or possibly areas with reversed remanent magnetization. In the same context, another pseudogravity low over the Nautilus Spur (L3) may also be sourced by a block of non-magnetized (or negatively magnetized) crust.

5. Geophysical transects of the Alpha Ridge

To investigate the crustal structure of the HALIP we have constructed 2-D forward gravity and magnetic models constrained by depth interfaces from seismic interpretations, velocity/density functions from sonobuoy analysis and wide-angle seismic refraction profiles.

In constructing these geophysical block models, we follow a minimalist philosophy (i.e., to use as few discrete bodies as possible to match the broad gravity and magnetic anomalies). The initial geometry of each model was constructed with the known seismic constraints along each transect. The models were extended over 500 km on either side to prevent edge effects in the calculated gravity and magnetic values. Density values were assigned to each block (see Section 5.1), and the model geometry was first modified to fit the gravity data since the bulk densities of the rock units are better constrained and large-scale changes are required to affect the long wavelength component of the gravity field (e.g. depth to Moho). Once an initial gravity-defined crustal geometry was developed, magnetization values were assigned to the model blocks, first assuming a simple induced magnetization with the geometry of the blocks defined by the gravity model, and then adding remanent magnetization as required. A magnetic field value of 57,500 nT, with a magnetic inclination of 90° and a declination of 0° (since we are close to the geomagnetic pole) were used for all models. Several iterations were made for each model until a geologically realistic solution was obtained. Gravity and magnetic modeling was carried out using GM-SYS (PRO)™ v.4.10.

5.1. Velocity–density conversion

As there are no deep-water drill holes in this part of the Arctic region, rock densities were assigned using sonobuoy interval velocities and an empirical velocity–density relationship of laboratory sample measurements (Ludwig et al., 1970).

This relationship is consistent with published (Vp) velocity–density values for basalts (e.g. Christensen, 1976, 1977; Christensen et al., 1974, 1979, 1980a,b; Salisbury and Christensen, 1976; Schreiber and Fox, 1977), serpentinites (e.g. Christensen, 1966, 2004; Courtier et al., 2004) and dredge samples collected from the USCGS Healy in 2009 (Salisbury, pers. comm., 2014). Although the 2009 USCGS Healy dredge samples were highly altered, and the measured Vp velocities were anomalously low for the respective lithologies (Salisbury, pers. comm., 2014), their Vp–rho relationships do fit the Ludwig et al. (1970) curve. The large range of Vp values for serpentinites (4.6 to 8.4 km/s) reflects the degree of alteration of the original mineralogy (e.g. olivine). The highest values represent 0% alteration and the lowest represent 100% alteration. Vp values for basalts range from 4.6 to 7.2 km/s and cannot be uniquely distinguished from serpentinized ultramafic rocks. For our gravity modeling, prior lithological interpretation is not required as all lithologies follow the same Vp–rho relationship. We only need Vp constraints to reasonably assign appropriate density values.

In Fig. 3 we show the Ludwig et al. (1970) Vp–density plot overlain with the basalt, serpentinite, and Healy dredge sample data mentioned above. The colour coding is the same as shown in the (Figs. 5 and 6) model results. For clarification, the velocity–density intervals have been summarized in Table 1.

5.2. Magnetization

Modeling the magnetic sources for the HAMH requires some ad hoc assumptions since there are no independent measurements of the deep magnetic properties of the high Arctic crust (i.e., no deep drill holes). Dredge samples collected aboard the USCGS Healy in 1990 on the northern portion of the Chukchi Plateau recovered six basalt samples (see Fig. 1 for locations). Although these samples are not within the HAMH domain, they provide some constraints on the magnetization of the

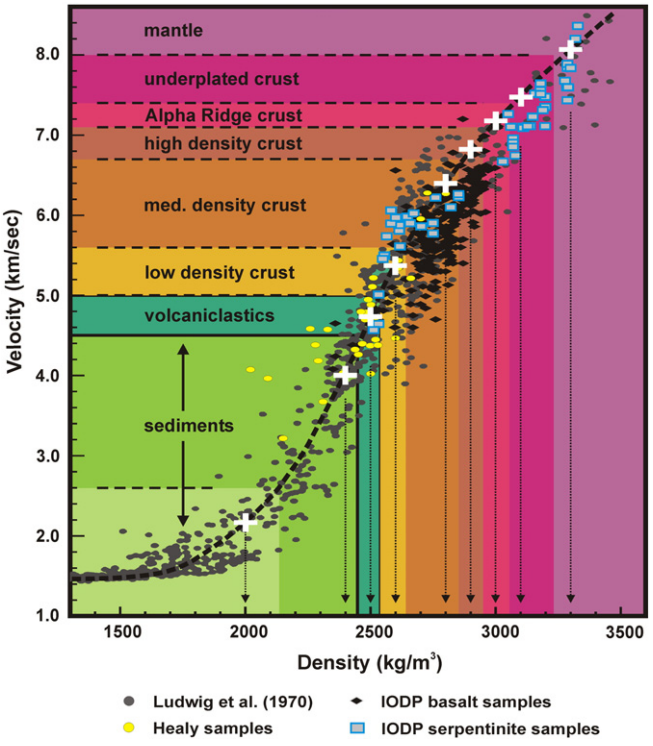

Fig. 3. P-wave velocity/density relationship for gravity modeling. P-wave velocities from wide-angle seismic lines (Forsyth and Mair, 1984; Forsyth et al., 1986a,b; Funck et al., 2011) and sonobuoy stations (Chian and Lebedeva-Ivanova, 2015) were used to assign density values for the gravity modeling based on an empirical relationship with velocities (Ludwig et al., 1970) (grey dots). This relationship is compared with published velocity–density values for basalts (e.g. Christensen, 1976, 1977; Christensen et al., 1974, 1979, 1980a,b; Salisbury and Christensen, 1976; Schreiber and Fox, 1977) (black diamonds), serpentinites (e.g. Christensen, 1966, 2004; Courtier et al., 2004) (grey squares) and dredge samples collected from the USCGS Healy in 2009 (Salisbury, pers. comm; yellow dots).

Table 1
P-wave velocities and associated densities used in the modeling.

Lithology	P-wave velocity range (km/s)	Density (kg/m^3)
Low velocity sediments	<2.6	2000
Medium velocity sediments	2.6 to 4.5	2400
High velocity sediments or volcanoclastics	4.5 to 5.0	2500
Low density (volcanic) crust	5.0 to 5.6	2600
Medium density crust	5.6 to 6.7	2800
High density crust	6.7 to 7.1	2900
Alpha Ridge crust	7.1 to 7.4	3000
Underplated crust	7.4 to 8.0	3100
Mantle	>8.0	3300

regional volcanic rocks. The susceptibility values for these samples ranges from 27 to 142 × 10^{-3} SI units (median value of 63 × 10^{-3}) (Salisbury pers. comm., 2014), fairly typical for basalts, and suggest that extremely high (induced) magnetization for a shallow and thin magnetic layer is not the cause of the high magnetic amplitudes within the HAMH.

The Cretaceous igneous rocks collected from the Canadian Polar Margin (Estrada et al., 2016) show a significant range of the magnetic susceptibility values. Rock samples from the Wooton Intrusive Complex vary between 0.7 and 68 × 10^{-3} SI units, and from the Hansen Point Volcanic Complex between 0.4 and 61 × 10^{-3} SI units.

To match observed anomaly amplitudes the magnetic models required some very high bulk magnetization values (>250 × 10^{-3} SI). Since these values exceeded the range of susceptibility measurements cited above, we included a combination of induced and normal remanent magnetization for some of the modeled magnetic bodies.

5.3. Simplified cross section/geologic cartoon (A1)

Transect A1 (Fig. 4) is a ~1600 km, gravity/magnetic cross section model that extends from the Canada Basin, across the Alpha Ridge, through the Makarov Basin to the Lomonosov Ridge (Figs. 1 and 2). For this model we take a generalized approach to demonstrate that a simplified source-body geometry is capable of matching the first-order features of the gravity and magnetic anomalies.

We model a simplified crust as a single layer with a density of 2800 kg/m^3 and a higher-density (3000 kg/m^3) beneath the Alpha Ridge. A 5-layer density model (water, sedimentary rocks, crust, crustal root, mantle) fits the free air gravity anomaly reasonably well (Fig. 4B). The shorter wavelength variations result simply from the bathymetric variations (i.e., the lateral density contrast of crustal rocks with water). The generally lower free air gravity over the Canada Basin results from the lateral density juxtaposition of oceanic sedimentary rocks with crystalline crustal rocks. The broad gravity swell over the Alpha Ridge is caused by the combined high of the long wavelength component of the Alpha Ridge with a compensating low caused by the crustal root.

We fit the magnetic anomalies (Fig. 4A) using a set of crustal blocks with varying magnetic intensities (a combined effect of induced and remanent magnetization). The magnetic data was upward continued by 10 km to emphasize bulk crustal features at the expense of noisy shallow variations. We chose to fix the top of these blocks to the top of the crystalline crust, fixed the magnetic intensity based on the overall amplitude of the magnetic anomalies in that zone, then inverted for the bottom geometry of the blocks. Of particular note is the presence of a source body with reverse polarity magnetization (−60 SU) corresponding to the large "Nautilus Spur" magnetic low between 600 and 750 km along the modeled transect (Fig. 4C). This magnetic low cannot be produced without reversed remanent magnetization. The tectonic implication is that the emplacement of this portion of the HALIP volcanics ranged over a time period which included a magnetic polarity reversal.

The resulting geologic model (Fig. 4D) is a conceptual illustration of the portion of the crust affected by a deep crustal dike and sill emplacement related to the HALIP. The highly magnetic blocks reflect the bulk effects of intruded and underplated mafic and ultramafic material related to the LIP event and support the interpretation that the total vertical dimension of intrusive/extrusive material in the upper crust ranges from about 5 to 10 km.

5.4. "Coupled" 2D modeling

An alternative method for modeling the gravity and magnetic anomalies is to use laterally continuous source-body layers with uniform density and magnetization values. Modeling is done by modifying the geometry of the layer interfaces to simultaneously fit both the observed gravity and magnetic anomalies. P-wave refraction velocities were used to constrain the assigned density values of the modeled layers (as defined by the Vp–rho relationship). Magnetization values assigned to each layer were modified experimentally to best fit the amplitudes and wavelengths of the observed magnetic anomalies. Since the gravity and magnetic fields obey different wavelength dependent depth-to-source relationships ($1/r^2$ for gravity and $1/r^3$ for magnetics), the different wavelengths of the observed data provide some constraints on the depths that modifications can be made to the model. This "coupled" approach minimizes the necessity of assigning arbitrary (and unconstrained) physical properties to the source bodies.

5.4.1. Axial profile (A2)

Transect A2 (Fig. 5) is a ~1200 km long profile extending from Axel Heiberg Island on the Canadian Polar margin along the long bathymetric axis of the Alpha Ridge. The near shore section of the profile coincides with the ~360 km long seismic refraction line of the ARTA experiment (Funck et al., 2011). Since this model is constrained by a large number of seismic receiver stations (with an average spacing of 1.4 km), it has a complex crustal geometry. A simplified version of the gravity model of Funck et al. (2011) was incorporated in our model. Moho depths from the CESAR "strike-line" seismic refraction profile (Asudeh et al., 1988) were used as preliminary constraints for the central portion of the model (~500 to 700 km). Sonobuoy velocities from Jokat et al. (2013) and Chian and Lebedeva-Ivanova (2015) were used to constrain the upper crustal density structure at the distal end of the profile. The A3 "cross-line" model intersects at ~820 km.

Over the continental platform and nearshore portion of the transect (0 to 300 km) the magnetic anomalies (Fig. 5A) have low amplitudes (−200 to +50 nT; typical of continental crust). High amplitude magnetic anomalies (−500 to 1500 nT) are observed along the entire length of the Alpha Ridge portion of the transect (within the HAMH).

Free air gravity anomalies along the A2 transect (Fig. 5B) are highly variable, with amplitudes ranging from ~−25 to +70 mGal. A mean gravity anomaly of ~+25 mGal suggests that the ridge is not in local isostatic balance (i.e., the crust has significant structural rigidity and isostatic support is distributed regionally).

Individual free air gravity highs correlate closely with bathymetric highs along this profile. The Bouguer corrected gravity removes most of the bathymetric correlation; however, a significant broad residual low Bouguer anomaly over the central portion of the profile (~−25 mGal) could indicate relatively lower deep crustal densities which could contribute buoyancy to regional isostatic compensation.

The continental portion (left side) of the model (Fig. 5C) includes a 2900 kg/m^3 lower crust and 2800 kg/m^3 upper crust. A mid-crustal moderately magnetic layer (5 × 10^{-3} SI) was required to fit the observed magnetic anomalies (Fig. 5D). Medium density (2500 kg/m^3) (Paleozoic and Mesozoic?) and (2400 kg/m^3) (Cenozoic?) non-magnetic sedimentary successions extend off the continental platform onto the slope regions of the margin.

Adjacent to the continental platform, the crust is modeled with a lower (2900 kg/m^3) non-magnetic layer and an upper (2600 kg/m^3)

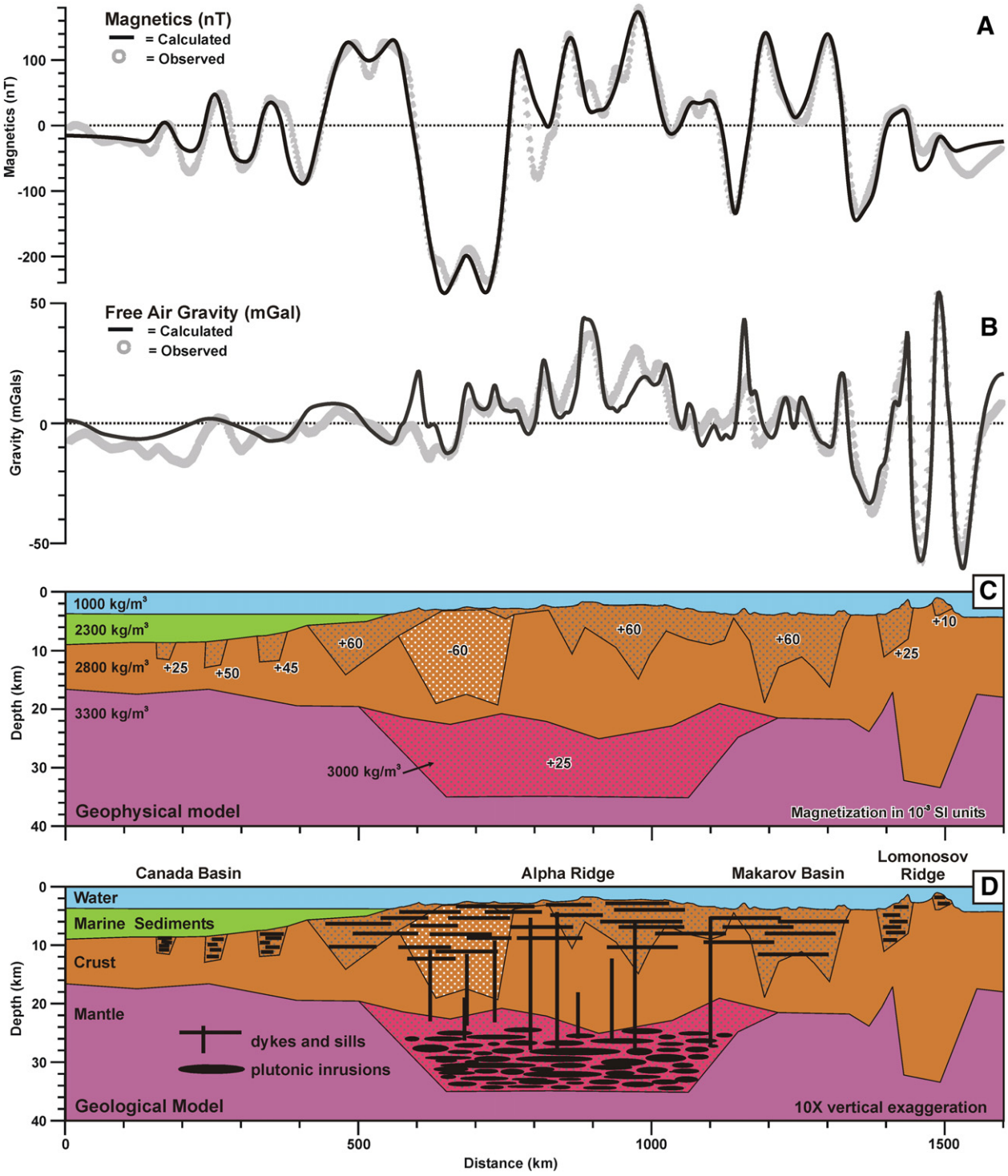

Fig. 4. Generalized profile/cartoon (A1). Geophysical block model (2D forward model) along transect A1 (location shown in Figs. 1 and 2). The top panel (4A) shows the observed and calculated regional magnetic field (upward continued by 10 km to emphasize crustal scale features). The second panel (4B) shows the observed and calculated free air gravity anomaly (as observed at sea level). Panel 4C shows the block model geometry. The black stippled areas are the positively magnetized blocks. The white stippled block has negative (reversed) magnetization. The bottom panel (4D) shows the geologic interpretation of the geophysical block model.

layer. Portions of this upper crustal layer required high magnetization (both induced and remanent). Funck et al. (2011) identified a high velocity (>7.5 km/s) (underplated) layer in this "transition" portion of the margin, which we modeled as a 3100 kg/m^3 layer. This layer does not appear to contribute significantly to the magnetic anomalies. A volcanoclastic layer (2500 kg/m^3) with moderate magnetization (25×10^{-3} SI, no remanent magnetization) is modeled from the outer edge of the "transitional zone" across all of Alpha Ridge. A thin low density (2000 kg/m^3), non-magnetic (Paleogene?) sedimentary layer drapes over all of the Alpha Ridge and onto the continental margin.

The Alpha Ridge portion of the transect was modeled with a thick (3000 kg/m^3) lower crustal layer, a mid crustal (2900 kg/m^3) layer, and an (2600 kg/m^3) upper crustal layer. Based on estimates of Curie temperature depths in this region (Taylor et al., 1986), all of the Alpha Ridge crust was considered magnetic. Most of the lower crustal layer was assigned moderate magnetization values (25×10^{-3} SI) with no

remanent magnetization (LC1). The mid- and upper-crustal layers were assigned high magnetization values (85×10^{-3} SI) as well as a significant remanent magnetization component (7 A/m; Fig. 5). As mentioned in Section 5.2, higher induced magnetization values could have been assigned to these layers; however, they would be inconsistent with measured laboratory values of typical volcanic rocks. Additionally,

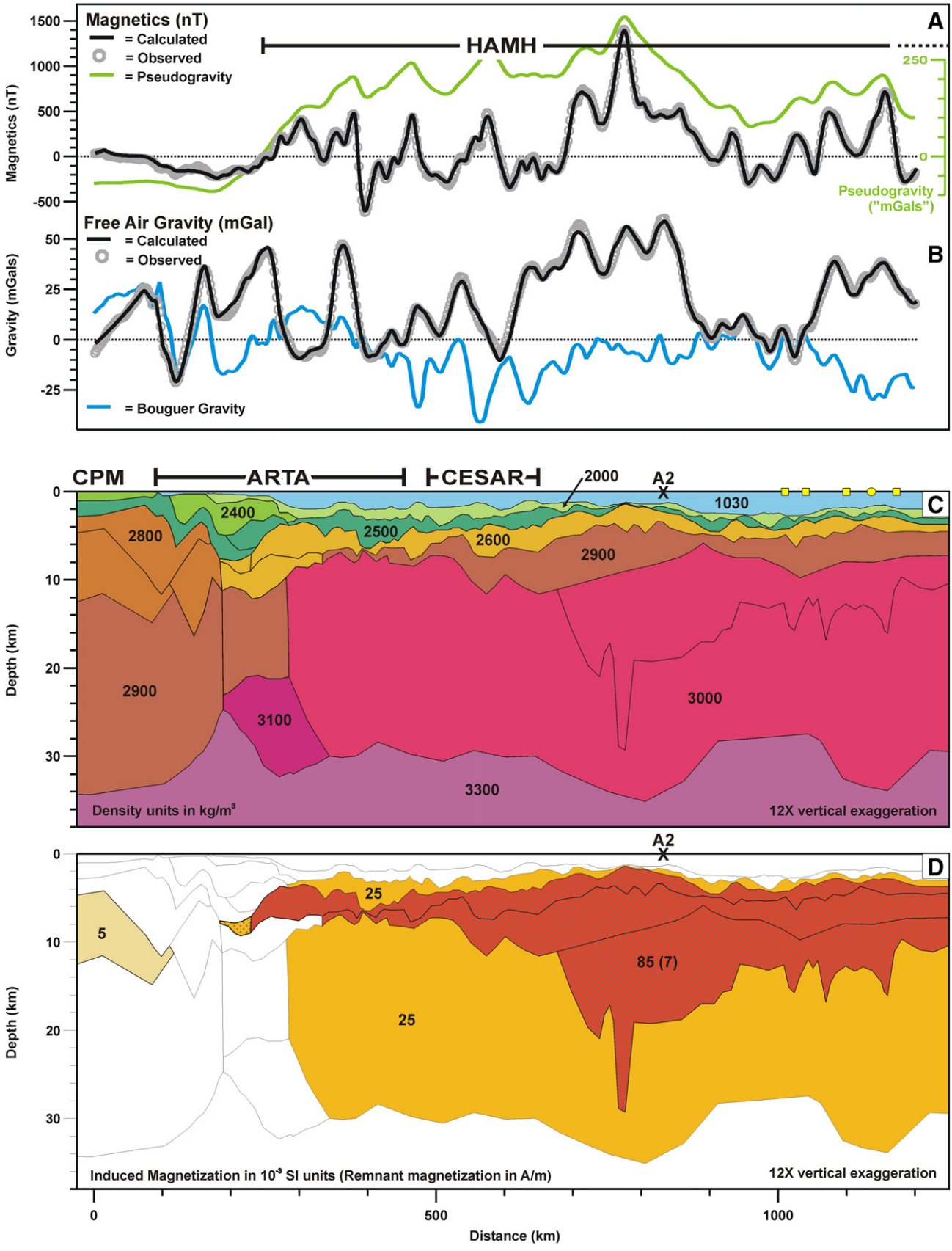

extremely high amplitude magnetic anomalies (beyond 700 km along the profile) cannot be modeled with shallow sources, and a significant portion of the lower crustal layer (LC2) also required a remanent magnetization component. The center of the "deep magnetic root" (at ca. 800 km) corresponds with the maximum value of the calculated pseudogravity (green profile).

A volcanoclastic layer (2500 kg/m^3 with moderate magnetization (25×10^{-3} SI, no remanent magnetization) is modeled across all of Alpha Ridge. This layer does not appear to onlap the "transition" portion of the margin. A thin (~1 km) low density (2000 kg/m^3), non-magnetic sedimentary layer extends from the continental margin across all of the Alpha Ridge.

Moho depths for the continental platform are 30 to 34 km and shallow abruptly to a minimum of ~28 km at the inner edge of the "transitional zone". Modeled Moho depths range between 28 and 35 km for most of the Alpha Ridge, with the deepest values (ca. 800 km) coincident with the position of the lower crustal magnetic root.

5.4.2. Alpha Ridge cross-line (A3)

The Alpha Ridge cross-line transect model (A3) is ~1400 km long and extends from the Canada Basin to the Amundsen Basin (Fig. 6). The crustal geometry of the Lomonosov Ridge is constrained by the LOREX seismic refraction line (Forsyth and Mair, 1984). The geometry of the upper crustal portion of the Alpha Ridge adjacent to the Canada Basin (ca. 0 to 450 km) is constrained by seismic reflection data collected by joint Canada/U.S. icebreaker operations (Mosher et al., 2009). Refraction seismic velocities from seven sonobuoy stations (Chian and Lebedeva-Ivanova, 2015) coincident with the seismic line were used to define the density values in the modeling. Although Chian and Lebedeva-Ivanova (2015) report Mantle reflection (PmP) and refraction (Pn) arrivals from some of the sonobuoy stations on the Canada Basin flank of Alpha Ridge, the quality of these deep arrivals is poor, and their Moho depth estimates (16 to 17 km) were used only as initial constraints in our models. The Axial transect model (A2) intersects at ~840 km.

For the entire extent of the Alpha Ridge cross-line, large amplitude (~−450 to +650 nT) magnetic anomalies (Fig. 6A) are observed. The largest amplitudes are between ca. 700 and 1050 km and correspond with the maximum values of the calculated pseudogravity at the axis of the Alpha Ridge.

The free air gravity anomalies along the A3 transect (Fig. 6B) are smaller on the Canada Basin flank of the Alpha Ridge (between ca. 100 and 400 km) with values ranging from ~−5 to +10 mGal. A zero mean value for this portion of the transect is consistent with local isostatic equilibrium. Between ca. 700 and 1050 km, the free air gravity anomalies have a much higher amplitude range (~−20 to +50 mGal) and a mean value of ~+15 mGal, which suggests that the central (axial) portion of the Alpha Ridge has significant structural rigidity (with regional isostatic compensation). A large free air gravity high (~70 mGal) is coincident with this portion of the Lomonosov Ridge. Similar to the Axial transect (A1), individual free air gravity highs correlate with bathymetric highs, which are (mostly) removed by the Bouguer correction. There are two notable exceptions: at ~400 km (over Nautilus Spur) and at ~1250 km (over Lomonosov Ridge). In both cases, the Bouguer correction (using 2670 kg/m^3) overcompensates, suggesting that the bathymetric highs consist of lower density material.

Two crustal layers were assigned to Amundsen Basin (2800 and 2900 kg/m^3). Only the upper layer was magnetic (25×10^{-3} SI induced and 7 A/m remanent magnetization). A medium density (2500 kg/m^3) magnetized (25×10^{-3} SI induced; no remanent component) volcanoclastic layer extends from the Canada Basin across Alpha Ridge and into the Makarov Basin. This layer does not extend across Lomonosov Ridge. It has a maximum thickness of ~2 km over the axis of Alpha Ridge. The Lomonosov Ridge was modeled with a (non-magnetic) lower crustal layer (2900 kg/m^3) and an upper crustal layer (2800 kg/m^3) with a moderate magnetization (50×10^{-3} SI induced; no remanence). Two non-magnetic, low-density sedimentary layers were included in the model. The thickness of the lower (2400 kg/m^3) layer ranges from ~2 to 4 km within the Canada and Makarov basins and only ~1 km within the Amerasia Basin. The thin (<1 km) upper layer (2000 kg/m^3) was modeled across all of the transect.

As with the Axial Transect (A2), the Alpha Ridge was modeled with a lower crustal layer (density of 3000 kg/m^3), a mid-crustal layer (density of 2900 kg/m^3), and an upper crustal (volcanic) layer (density of 2600 kg/m^3) (Fig. 6C). Both the mid-crustal and upper crustal layers required high magnetization values (85×10^{-3} SI induced and 7 A/m remanent). The lateral extent of these highly magnetic layers corresponds with the HAMH defined by the pseudogravity. The (combined) mid- and upper-crustal layers of the Alpha Ridge range from ~5 to 8 km and are thickest on the Canada Basin flank. Most of the lower crustal layer (LC1) was assigned moderate magnetization values (25×10^{-3} SI induced) (Fig. 6D); however, the uppermost 6 to 8 km (LC2) required high magnetization values (both 85×10^{-3} SI induced and 7 A/m remanent). The model shows a large variability in interface depths between LC1 and LC2 beneath Nautilus Spur — i.e. large (deep) lateral magnetization contrasts are required to fit the amplitudes and wavelengths of the observed magnetic anomalies. This could alternatively be modeled with localized source-bodies having either extremely high magnetization or reversed remanent magnetization. We preferred to maintain a simple approach and minimize the variability in the physical properties of the source bodies. In detail, the model is only able to identify that there is a complex magnetization structure and cannot resolve internal compositional and structural detail.

The (oceanic?) crustal layer in Canada Basin (density 2800 kg/m^3) required moderate magnetization values (25×10^{-3} SI). The high density underplated layer (3100 kg/m^3) modeled beneath the Canada Basin flank of Alpha Ridge was based on the sonobuoy velocities (>7.5 km/s). Whether this layer is a persistent feature beneath Alpha Ridge is unknown and would require supporting refraction seismic data to include in the modeling.

The maximum modeled Moho depth beneath the Alpha Ridge (~31 km) is at ca. 880 km, approximately at the intersection with the (A2) Axial transect. Moho depths shallow towards the Makarov Basin to a minimum depth of ~12 km. Towards the Canada Basin, Moho depths shallow (but much more gradually) to a depth of ~23 km at ca. 500 km. There is a notable "crustal root" beneath the Nautilus Spur, where a local Moho depth of ~26 km is calculated. The minimum Moho depth at the base of Alpha Ridge lower crustal layer (LC1) is ~18 km at ca. 300 km. Moho depths at the base of the underplated layer (on the Canada Basin flank of Alpha Ridge) are between ~12 and 16 km — slightly less than the 16 to 17 km depth estimates from the sonobuoy data (Chian and Lebedeva-Ivanova, 2015).

Fig. 5. Alpha Ridge axial profile (A2). Detailed geophysical profile model extending from the Canadian Polar Margin (Axel Heiberg Island) along the bathymetric axis of Alpha Ridge (Profile A2 on Figs. 1 and 2). Synthetic profiles of bathymetry (Jakobsson et al., 2012); free air gravity (Andersen et al., 2010) and magnetic anomalies (Gaina et al., 2011) were extracted from the published grids for the modeling. 5A shows the observed and calculated magnetic anomalies and the pseudogravity anomaly (green line). 5B shows the observed and calculated free air gravity anomalies and the marine Bouguer anomaly (blue line). 5C shows the geometry density parameters used in the gravity modeling. 5D shows the geometry magnetization parameters used in the magnetic modeling. The locations of the wide-angle refraction seismic constraints are shown on panel 5C (ARTA: Funck et al., 2011; CESAR, Asudeh et al., 1988). Also shown are the sonobuoy station positions (yellow squares from Jokat et al., 2013; yellow dot from Chian and Lebedeva-Ivanova, 2015) and the intersection location of the A1 model. CPM = Canadian Polar Margin; LC1 = moderately magnetized lower crust; LC2 = highly magnetized lower crust.

5.5. Summary of the geophysical transects: volume of the HALIP

For the detailed Axial (A2) and cross-line (A3) models (Figs. 5 and 6), we show that the Alpha Ridge can be modeled with a simple three-layer crustal structure. Although there are minor differences in the geometries of the A2 and A3 models where they cross, we believe this to be an inherent limitation of 2-D modeling of 3-D structures.

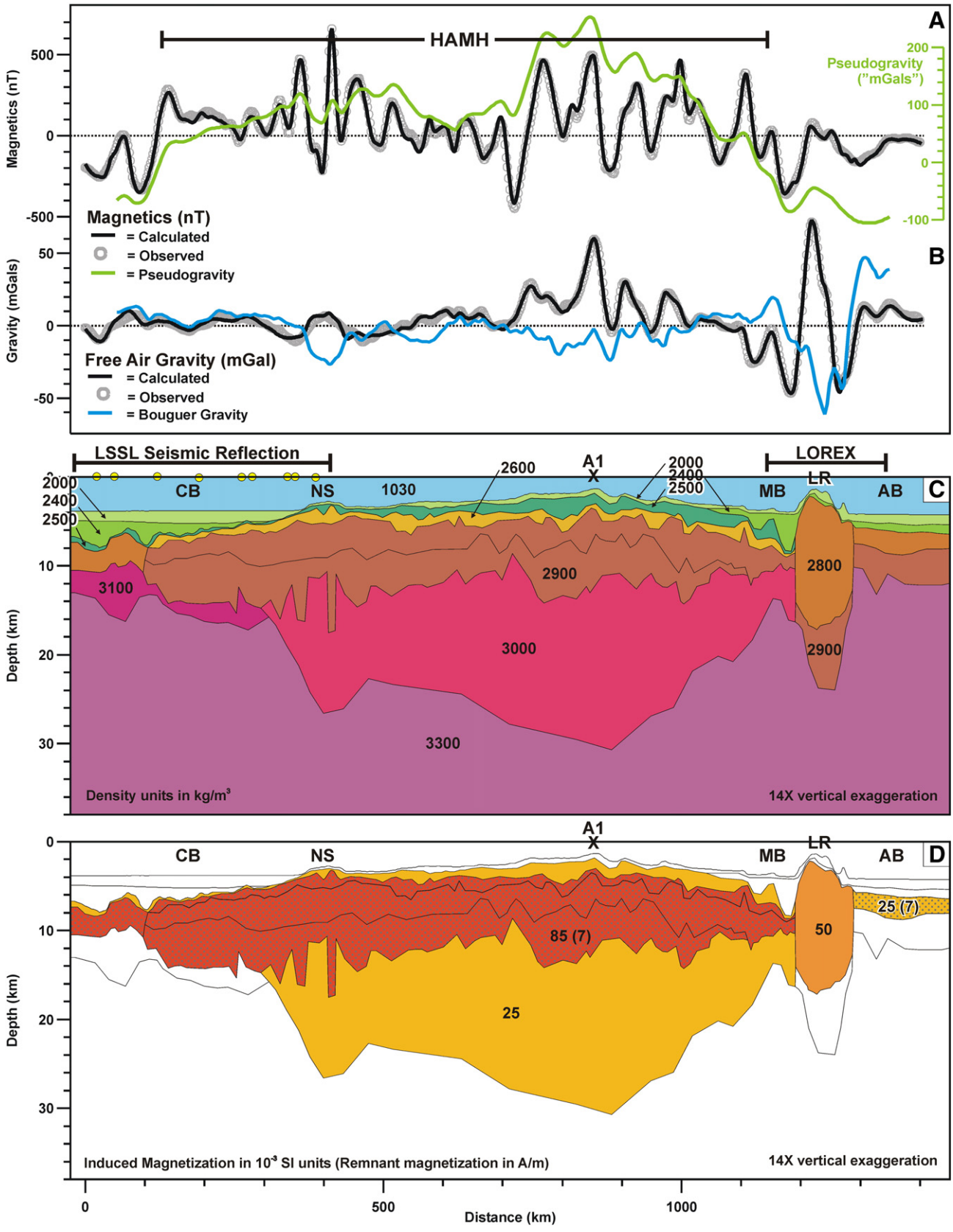

Very high magnetization values were needed for upper portions of the lower crust (LC2), as well as the mid- and upper-crustal layers. Since the values needed in the models exceeded typical susceptibility values of volcanic rocks, we concluded that there was a significant component of normal remanent magnetization. Emplacement of the bulk of the Alpha–Mendeleev volcanic complex during the C-34 Cretaceous "super-chron" (124 to 84 Ma) would explain the persistence of normal polarity remanent magnetization. Evidence of reverse-polarity remanent magnetization beneath Nautilus Spur (on model 3) suggests that volcanism may have spanned a longer time range to include times before and/or after chron C-34.

The 2900 kg/m^3 mid-crustal and 2600 kg/m^3 upper-crustal layers are interpreted as the combined effect of sills, dikes, and flows resulting from a (plume-sourced) LIP intrusion. Assuming that the (combined) thickness of the mid- and upper-crustal layers (5 to 10 km) is representative over the entire HAMH (and the aerial extent of 1.3×10^6 km^2) a volumetric estimate of (at least) 6×10^6 km^3 is calculated for the volcanic upper crust.

The thick 3000 kg/m^3 lower crustal layer is interpreted as a composite of the protolithic crust and deep (ultramafic) plutonic intrusions related to a mantle plume. The density of 3000 kg/m^3 is atypical of either oceanic or continental crust. If we assume an oceanic protolith (with a density of 2900 kg/m^3), the ultramafic component (density of 3100 kg/m^3) represents ~50% of the layer by volume. Using our modeled thickness of the lower crust as typically over 20 km, the original oceanic protolith would have been ~10 km thick — reasonable for typical oceanic crust. If instead we assume a continental protolith (with a density of 2800 kg/m^3) the resulting ultramafic intrusive volume exceeds 65% and implies an original crustal thickness of ~7 km — consistent with estimates of "hyper-thinned" continental crust within Canada Basin (Chian et al., 2016). Using the aerial extent of the HAMH and a range of 50% (oceanic protolith) to 65% (continental protolith) volcanic intrusive content within the (~20 km thick) lower crust, we calculate volumetric estimates of between 13×10^6 and 17×10^6 km^3. Although the ARCTIC2000 refraction line (Lebedeva-Ivanova et al., 2006) identified the presence of high-velocity underplating beneath the Mendeleev Ridge, our models do not include a broadly distributed (high density) underplated volcanic crustal layer beneath Alpha Ridge. As such, a volumetric estimate of the underplated material is difficult to make.

In summary, we estimate the total volcanic component of the Alpha–Mendeleev portion of the HALIP to be between 19×10^6 km^3 and 23×10^6 km^3.

6. Comparison of the HAMH magnetic anomalies and pseudogravity with global analogs

The magnetic anomalies and pseudogravity of four global LIPs are shown in Fig. 7 to illustrate analogs for the HAMH. Although there are many other possible global analogs, these examples have been chosen in part because of their geological variability, and because of the adequate quality of regional magnetic coverage (necessary for calculating pseudogravity). Magnetic data for the Siberian Traps and Kerguelen Plateau are from the global EMAG2 compilation (Maus et al., 2009). The magnetic data for the Columbia Flood Basalts are from the North American NAMAG compilation (Bankey et al., 2002). Magnetic data for the North Atlantic Igneous Province are from the Atlantic–Arctic GAMMAA5 Verhoef et al. (1996) compilation.

6.1. Siberian Traps

The Siberian Traps are a large volcanic complex in central and northern Siberia consisting of early Triassic extrusive and intrusive basalts (Fig. 7A). The central extrusive flood basalts cover an area of ~7×10^5 km^2. Extensive dikes and sills intruded the regional Paleozoic successions and are exposed in a broad area around the central extrusive complex. Also, outliers of extrusive flood basalts are exposed to the south in the Kuznetsk Basin, and to the west at Vorkuta at the northern end of the Ural Mountains. Structurally emplaced basalts also outcrop along the southern edge of the Taimyr Peninsula. To the west of the central extrusive complex, basalts have been sampled from several wells below the Mesozoic and Cenozoic strata of the West Siberian Basin and isolated volcanic centers correlate with the geometry of major extensional fault systems within the basin (Reichow et al., 2009). The total area of the Siberian Trap volcanic province exceeds 5×10^6 km^2.

The magnetic anomalies over the central extrusive complex (Fig. 7A) have moderate amplitude high frequencies with a general chaotic character, similar to the HAMH. This pattern does not continue over the "intrusive rim" surrounding the central complex. Surprisingly, considering the large aerial extent and volume of the flood basalts, the pseudogravity anomaly high is localized only within the middle of the central complex. This suggests that the deep crustal portion of this complex has a limited extent. Over the West Siberian Basin, elongated magnetic highs correlate closely with the fault-bounded centers of the mapped volcanics. There pseudogravity shows large areas of positive amplitudes, suggesting that the aerial extent of the concealed volcanics within the basin may be much larger than the mapped exposures.

6.2. Columbia River flood basalts

The Neogene Columbia River Flood Basalt Province of Pacific Northwest United States covers an area of ~2.2×10^5 km^2 (Fig. 7B). The province is broadly subdivided into the Oregon Plateau and the Columbia Basin. The southern edge of the province is coincident with the Snake River Plain which follows the Yellowstone mantle plume hotspot track. Although volcanism related to this system started initially in the southern Oregon Plateau, the Columbia Basin became the ultimate epicenter of the flood basalts with a maximum thickness of over 4 km (Reidel et al., 2013).

Similar in character to the Siberian Traps, the short-wavelength magnetic anomalies over the central extrusive complex have moderate amplitudes with a chaotic character. From the magnetic character alone, there is little difference between the anomalies within the Columbia Basin and Oregon Plateau; however, the calculated pseudogravity values are significantly different. The large positive pseudogravity high over the Oregon Plateau (suggesting a deeper crustal root) extends much further west of the Oregon Plateau and corresponds with a deep magnetic source. The Snake River Plain "hot-spot track" corresponds with a linear belt of short wavelength positive magnetic anomalies and a linear pseudogravity high. This is expected since the plume source would presumably have influenced the entire thickness of continental crust.

6.3. North Atlantic Igneous Province

The North Atlantic Igneous Province (NAIP) includes widespread early Tertiary continental flood basalts and seaward-dipping flows

Fig. 6. Alpha Ridge cross-line profile (A3). Detailed geophysical profile model from the Canada Basin to the Alpha Ridge and into the Eurasia basin (Profile A2 on Figs. 1 and 2). Synthetic profiles of bathymetry (Jakobsson et al., 2012); free air gravity (Andersen et al., 2010) and magnetic anomalies (Gaina et al., 2011) were extracted from the published grids for the modeling. 6A shows the observed and calculated magnetic anomalies and the pseudogravity anomaly (green line). 6B shows the observed and calculated free air gravity anomalies and the marine Bouguer anomaly (blue line). 6C shows the geometry density parameters used in the gravity modeling. 6D shows the geometry magnetization parameters used in the magnetic modeling. The locations of the seismic reflection data (LSSL line Mosher et al., 2009), the sonobuoy seismic refraction stations (Chian and Lebedeva-Ivanova, 2015; yellow dots), and the LOREX wide-angle seismic line (Forsyth and Mair, 1984) are shown on panel 6C. The intersection location of the A2 model is also shown. AB = Amundsen Basin; CB = Canada Basin; MB = Makarov Basin; NS = Nautilus Spur; LC1 = moderately magnetized lower crust; LC2 = highly magnetized lower crust.

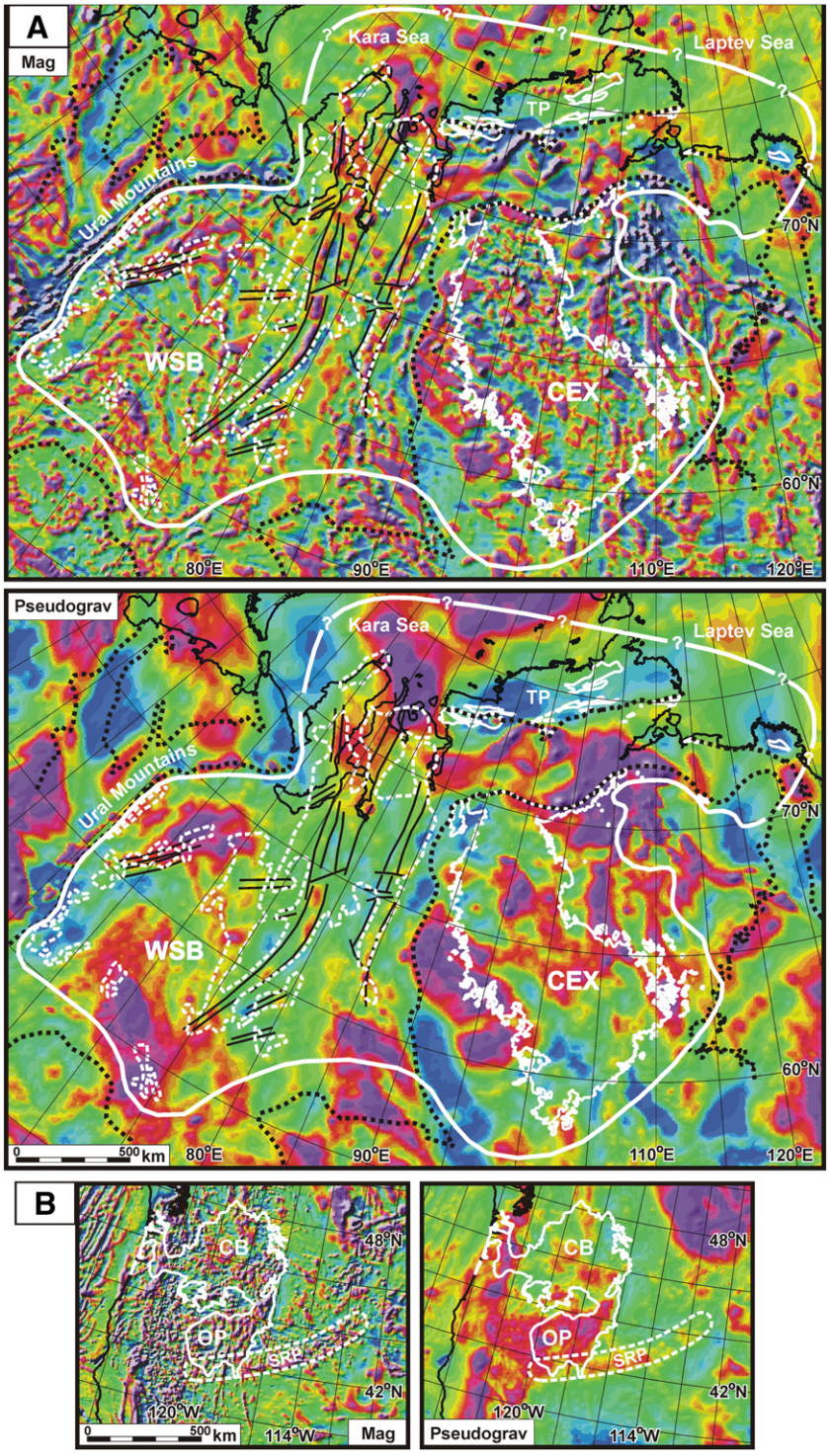

Fig. 7. Global LIP analogs (magnetic anomaly and pseudogravity). Comparison of magnetic anomaly patterns and pseudogravity of four global LIPs. Data sources are listed for each region. Pseudogravity was calculated using the same parameters as the HAMH. All maps are plotted at the same scale and use the same colour palettes as Fig. 2C and D. 7A) Siberian Traps. Magnetic data of the Siberian Traps region are from the global EMAG2 compilation (Maus et al., 2009). The outline of the extrusive complex (CEX; thin white lines) and edges of the Mesozoic–Cenozoic basins (dotted black lines) are from the International Polar Year circum-Arctic digital geology compilation (Harrison et al., 2011). The aerial extent of the Siberian Traps (thick white lines), structural elements (thin black lines) within the West Siberian Basin (WSB), and distribution of buried volcanics (dashed white lines) within the WSB are adapted from Reichow et al. (2009). The northern offshore extension of the Siberian Traps province is speculative. 7B) Columbia River Flood Basalts. Magnetic data covering the Columbia River Flood Basalt Province are from the NAMAG compilation (Bankey et al., 2002). The outline of the volcanic province (thick white line) is adapted from Reidel et al. (2013). A simplified outline of the Snake River Basin (SRB) (dotted white line) corresponds with the Yellowstone hot-spot track. The Columbia River Flood Basalt Province is subdivided into the southern Oregon Plateau (OP) and the northern Columbia Basin (CB). 7C) North Atlantic Volcanic Province (NAIP). Magnetic data for the Icelandic region of the North Atlantic is from the Verhoef et al. (1996) GAMMAA5 compilation. The outline of the NAIP (thick white line) is based (primarily) on the calculated pseudogravity anomaly and includes the onshore exposures of Cenozoic volcanics from the geology map of Greenland (Escher and Pulvertaft, 1995) and estimates of the extent of volcanics in the offshore areas off East Greenland and the European margin (Coffin and Eldholm, 1994). The 1000 m bathymetric contours are shown (thin black lines). GFR = Greenland–Faeroes Ridge; GP = Geikie Plateau; IC = Iceland; JM = Jan Mayen micro-plate; VMH = Vøring Marginal High. 7D) Kerguelen Plateau. Magnetic data for the Kerguelen Plateau region are from the global EMAG2 compilation (Maus et al., 2009). The outline of the Kerguelen Plateau (thick white line) is from Frey et al. (2000). The 1000 m bathymetric contours are shown (thin black lines). EB = Elan Bank; KI = Kerguelen Islands.

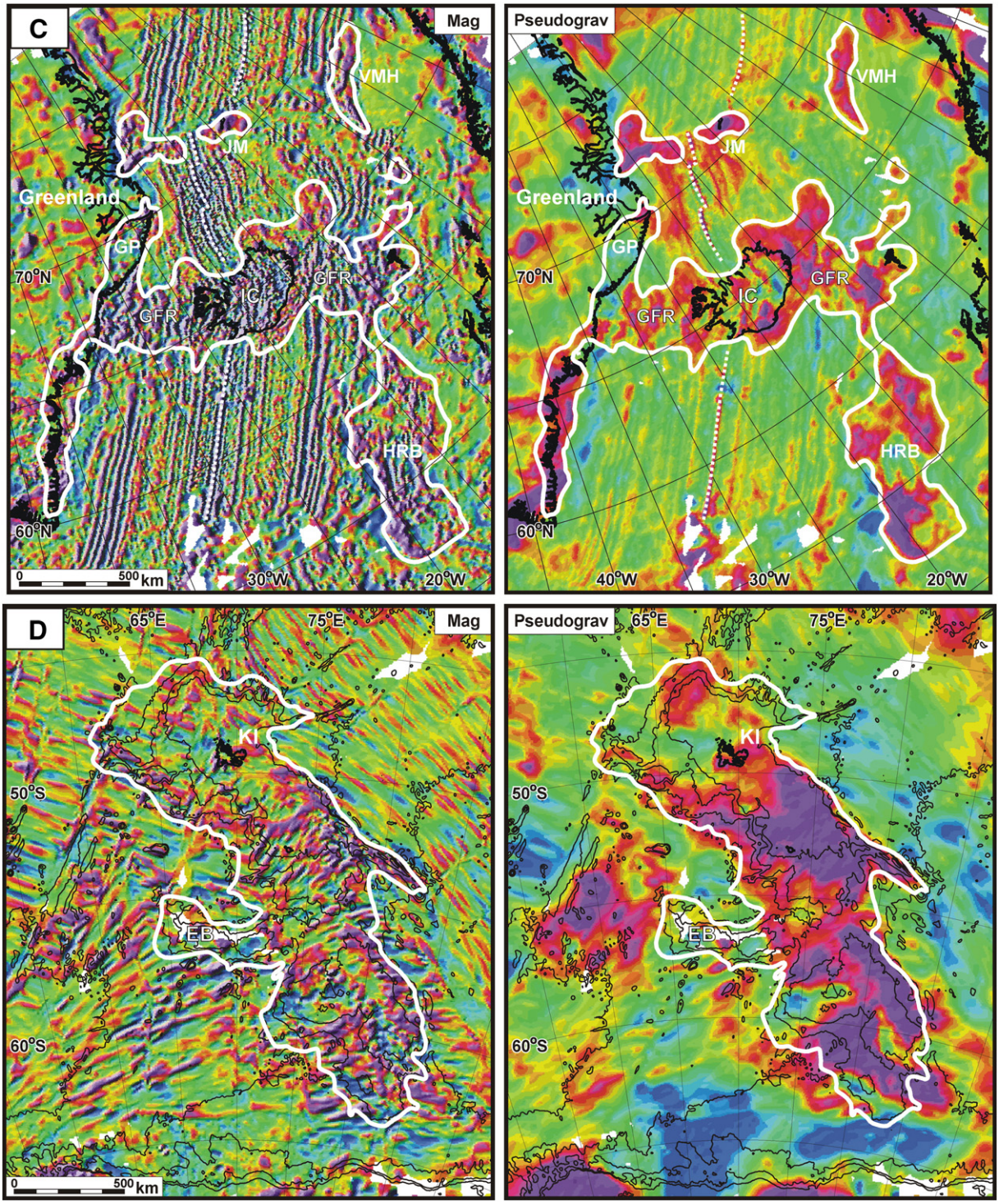

Fig. 7 (*continued*).

along the conjugate East Greenland and European margins (Fig. 7C). Excess volcanism is attributed to the influence of the Iceland Plume (e.g., Foulger, 1988; White, 1989; Clift et al., 1995), which maintained (approximately) a position coincident with the oceanic spreading ridge and formed the Greenland–Faeroes Ridge during the opening of the North East Atlantic. Lundin and Doré (2005), however, argue that a fixed plume (relative to the Earth's core; Müller et al., 1993) is inconsistent with producing the age-symmetry of the Greenland–Faeroes Ridge and that "hotspot drift" exactly matching the position of the oceanic spreading ridge is unlikely. The aerial extent of the North Atlantic volcanic province (including Iceland and the Greenland–Faeroes Ridge) exceeds 1.3×10^6 km^2 (Coffin and Eldholm, 1994).

At the northern extent of the NAIP isolated high amplitude magnetic anomalies on the Northeast Greenland shelf, the Jan Mayen Microplate and the Vøring Marginal High off the Norwegian coast correspond with positive pseudogravity anomalies. High amplitude short-wavelength magnetic anomalies and a large positive pseudogravity anomaly associated with the Greenland–Faeroes Ridge implies a deep source. Despite

extensive flood basalts on the Geikie Plateau, there are no high amplitude short-wavelength magnetic anomalies or positive pseudogravity anomaly in that region suggesting a thin or absent crustal root.

6.4. Kerguelen Plateau

The Kerguelen Plateau (Fig. 7D) in the southern Indian Ocean is defined primarily as a large regional bathymetric high. The plateau is considered a fragment rifted from the Gondwana supercontinent (125–100 Ma ago; Nicolaysen et al., 2000; Frey et al., 2000) that was later influenced by mantle plume volcanism (Bascou et al., 2008). Drill cores from OPD leg 183 recovered tholeitic basalts from the southern portion of the plateau and alkali basalts from the central plateau with age dates ranging from 109.5 to 114 Ma (Whitechurch et al., 1992). All samples had large geochemical and isotopic variations, suggesting continental crustal contamination. Garnet–biotite gneisses were sampled from Elan Bank confirming the presence of continental crust within the plateau. Upper Paleogene to Quaternary intrusive flood basalts and alkaline volcanic complexes are exposed onshore in the Kerguelan Islands (Nicolaysen et al., 2000) indicating active (plume related) volcanism. The areal extent of the Kerguelen Plateau is over 1.3×10^6 km^2 (Frey et al., 2000).

There is a large short wavelength positive magnetic anomaly pattern over most of the plateau, except northwest of the Kerguelen Islands where there is a magnetic low. The northwest–southeast magnetic lineations northeast of the plateau are seafloor spreading anomalies. The northeast–southwest magnetic lineations southwest of the plateau are possible gridding artifacts in the EMAG2 compilation. Very large high amplitude positive pseudogravity characterizes most of the plateau implying a deep crustal root. There is no positive pseudogravity northwest of the Kerguelan Islands which may mean that the extent of the volcanics does not include all of the bathymetric high, or that they have strong reverse remanence. A large positive pseudogravity anomaly west of Elan Bank may represent a continuation of the volcanic province beyond the bathymetric expression.

6.5. Overview of LIP comparisons

Our comparisons of the HAMH with magnetic analysis of the global LIP analogs show many similarities. All are generally characterized by high amplitude "chaotic" magnetic anomalies; however, there is a significant variability in the pseudogravity anomalies, which are interpreted to be the result of differences in the depths of the "magnetic root". Continental flood basalt provinces do not exhibit a large positive pseudogravity anomaly over the entire LIP area, which implies that despite the large volumes of extruded volcanics, the "deep plumbing" of the magnetic sources are localized mid- and lower-crustal features. Both continental and oceanic plume tracks show a positive pseudogravity anomaly signature (implying deep crustal extent). Of the four analogs we have presented, the Kerguelen Plateau shows the closest similarity of the size and character of the magnetic and pseudogravity anomalies of the HAMH.

7. Implications for arctic tectonics/geodynamics

LIPs have been correlated with global-scale events including sea-level rise and mass extinctions (e.g. Sobolev et al., 2011). Stratigraphic sections throughout the Arctic (Fig. 8) show significant unconformities at approximately 130 Ma and 85 Ma (Embry, 1989; Houseknecht and Bird, 2011; Hegewald and Jokat, 2013). As discussed in Section 2.1, volcanics from high Arctic regions associated with the HALIP (e.g. Tarduno, 1998; Maher, 2001; Andronikov et al., 2008; Mukasa et al., 2009, 2015; Brumley et al., 2013, Kingsberry et al., 2014; Petrov et al., 2015) show two main pulses of magmatism, one ranging from about 130–120 Ma, with a peak age at about 125 Ma (Corfu et al., 2013), and a younger episode from 90 to 80 Ma. Ernst and Bleeker (2010) point out the correlation and apparent causality of LIP initiation with tectonic breakup events and speculated that the circa 130 Ma initiation of the HALIP marks the initiation of the Amerasian Basin. Gaina et al. (2014) noted that the HALIP region was "potentially aligned with a favorable mantle plume source region at 130 Ma".

We find it difficult to understand how a single plume-related event would have had a 30 Ma hiatus in volcanism, and consider instead that the HALIP may have resulted from a multi-stage history of formation, consistent with the two sequence boundaries: the first phase involving the interaction of a mantle plume and the second with other tectonic or mantle events (e.g., convection), as suggested by several authors (e.g. Shephard et al., 2013; Lobkovsky, 2015; Saltus and Oakey, 2015). A multi-stage history has also been suggested for the Columbia Plateau (Hales et al., 2005). Based on the (limited) age-dated samples, volcanism on the Mendeleev Ridge is much older (260 Ma to 127 Ma; Morozov et al., 2013a,b) than the Alpha Ridge and Chukchi Borderlands (112 to 73 Ma; Jokat et al., 2013; Brumley, 2014; Mukasa et al., 2015). Whether there is a systematic (spatial) age distribution of volcanism or whether the two phases of volcanism overlap cannot be resolved with the existing data and more in-situ (i.e. drilling) samples are needed.

Fundamental questions remain regarding the crustal character of the Alpha–Mendeleev region prior to formation of the HALIP. Was the HALIP intruded into an existing oceanic or continental plate, or was it formed in a mid-ocean ridge setting?

Several lines of evidence suggest that the Alpha–Mendeleev region formed, at least in part, above sea level. Weber (1990) speculated, based on isostatic and thermal cooling considerations, that the Alpha Ridge was at least 1 km above sea level upon formation. Numerous authors (e.g., Embry, 1989; Midtkandal and Nystuen, 2009), have cited the need for a central Arctic sedimentary source region (termed "Crockerland" by Embry) for Cretaceous and later sedimentary sequences around the Arctic margins.

Assuming a single mantle plume model for the origin of the HALIP, our volume estimate for the source of the HAMH would form a sphere (plume head) with a diameter of about 300 km. By comparison with volumetric estimates derived for the Reunion (Deccan Traps) and the Iceland (North Atlantic Igneous Province) hotspots, we should expect a basal temperature differential of 200–250 °C (Sleep, 1990) and an energy flux into the base of the crust of 1–2 MJ/s (Sleep, 1990). The heat flux of this magnitude would raise the steady-state crustal conductive geotherm by at least 4 mW/m^2. This amount of heat input would cause a thermal change in both lithospheric mantle and crustal density and, along with the buoyancy effect of the hot asthenospheric material, would cause a broad surface uplift of at least 1 km for about 10–20 Ma following plume head arrival (consistent with estimates for the Reunion Hotspot; Sleep, 1990).

Analysis of sonobuoy velocity profiles throughout the Canada Basin (Chian and Lebedeva-Ivanova, 2015; Chian et al., 2016) suggests that only a relatively small central portion of the Canada Basin has crustal velocity profiles consistent with "normal" oceanic crust. They (Chian et al., 2016) interpret the Canadian Basin margin of the Alpha–Mendeleev ridge complex as "transitional" crust with high lower crustal velocities consistent with mantle serpentinization or deep mafic underplating of originally continental crust. This result suggests that the Canada Basin portion of the HALIP may have a continental protolith.

We further support the position that the Alpha Ridge was the result of the HALIP largely or completely intruding into continental crust. Our gravity/magnetic/bathymetric crustal cross section models are consistent with (but not absolutely diagnostic of) originally continental crust that has been massively intruded (and locally underplated) by LIP-related mafic material. In our interpretation the magnetic anomaly patterns of the HAMH are primarily related to the HALIP and it is difficult to "see through' the HALIP-related patterns to discern any prior crustal character. The relatively small Bouguer corrected gravity anomalies for the HAMH region, are consistent with a generally homogenous bulk crustal density

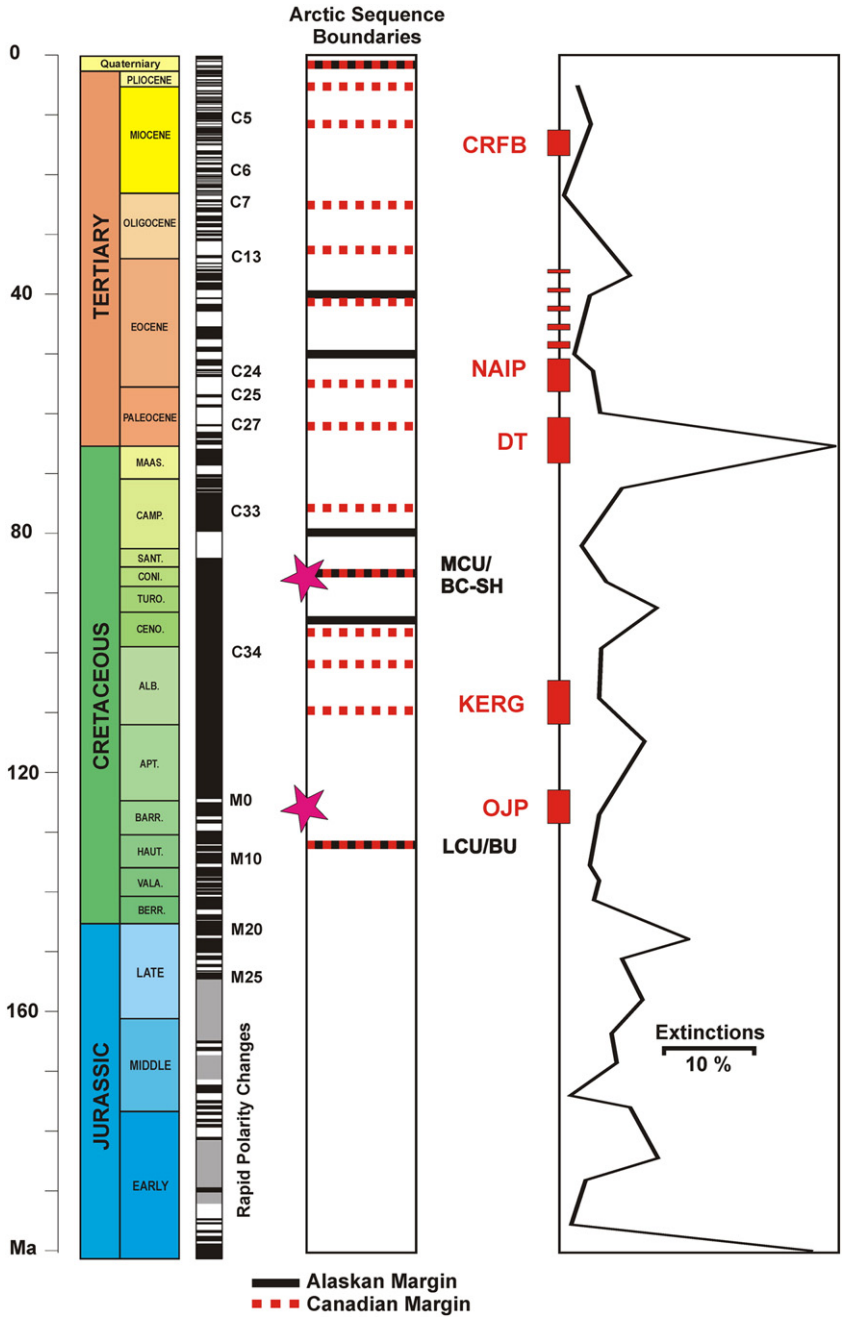

Fig. 8. Stratigraphic age correlations. Time chart of Arctic mega-sequence boundaries (adapted from Embry, 1989; Houseknecht and Bird, 2011), extinctions (Sobolev et al., 2011), and timing of major LIP events (Coffin and Eldholm, 1994). Stratigraphic chart and magnetic time scale are from Walker and Geissman (2009). Two major sequence boundaries are present in both the Alaskan and Canadian margin records: the Lower Cretaceous Unconformity/Breakup Unconformity (LCU/BU) at about 130 Ma and the "mid-Campanian/Boundary Creek-Smoking Hills" boundary (MCU/BC-SH) at about 85 Ma. These events coincide broadly with reported dates on major Arctic basaltic events (125 and 90 Ma; magenta stars). CRFB = Columbia River Flood Basalts; DT = Deccan Traps; KERG = Kerguelen Plateau; NAIP = North Atlantic Igneous Province; OJP = Ontong-Java Plateau.

which we attribute to the pervasive influence of the HALIP-related intrusions. Again, similar to the magnetic situation, it is difficult to see past the HALIP influence to reconstruct the gravity expression of the pre-existing crust. If the HALIP region was originally sub-aerial as inferred by some authors (e.g., Weber, 1990), it implies, even with the ~1 km thermal uplift expected, that the pre-HALIP crust was at or near sea level, consistent with a protolith of continental crust.

8. Conclusions

Recent international scientific interest has resulted in an unprecedented amount of new geophysical and geological data acquisition in the Arctic. With the increasing availability of large-scale public domain data compilations (e.g. Verhoef et al., 1996; Bankey et al., 2002; Pavlis et al., 2008; Maus et al., 2009; Andersen et al., 2010; Gaina et al., 2011; Harrison et al., 2011; Jakobsson et al., 2012; Chian and Lebedeva-Ivanova, 2015), we now have an enormous resource for quantifying the geological structure and tectonic framework of the Amerasia Basin. In this study, we have applied some basic magnetic and gravity data processing and interpretation techniques to define the first-order characteristics of the Alpha–Mendeleev ridge complex.

Free air gravity highs and lows generally correlate with the bathymetric relief. A mean free air gravity value of ~20 mGal over the

complex suggests that the structure is not in local isostatic equilibrium, and must be regionally compensated. The residual marine Bouguer gravity anomalies show no significant variation over the Alpha–Mendeleev ridge complex, which implies minimal lateral variability in the density structure. The magnetic anomalies show a region of high amplitude "chaotic" patterns (caused by broadly distributed volcanic rocks) that span the entire Alpha–Mendeleev ridge complex and extend beneath the sedimentary cover of the adjacent Canada Basin and the Makarov–Podvodnikov basins. Saltus et al. (2011) described this region as the "F1: Alpha–Mendeleev LIP magnetic domain". We have adopted a more generic term: the "High Arctic Magnetic High" (HAMH). The calculated pseudogravity (magnetic potential) inversion shows a regional positive high that represents the region with a deep (volcanic/magnetic) crustal root. The aerial extent of the HAMH is defined by a closed contour (isoline) of the pseudogravity and covers an area of ~1.3×10^6 km^2 — slightly smaller than the Saltus et al. (2011) "F1 Domain" (~1.5×10^6 km^2). Our new HAMH boundary onlaps the Canadian Polar Margin ("outcropping" onshore northern Ellesmere Island) and extends into the Makarov Basin approximately along the axis of Marvin Spur. We believe that Marvin Spur may be a volcanic ridge emplaced along the edge of the HALIP. Although there are magnetic highs along the flank of Lomonosov Ridge (near the Canadian Polar Margin), it is not included in the HAMH (i.e., deep-rooted HALIP volcanism did not affect the bulk crustal structure there).

A simple 3-layer igneous crust has been satisfactory for forward 2D gravity/magnetic modeling. Bulk crustal densities for the lower crust (3000 kg/m^3) are significantly higher than typical continental or oceanic crust and can only be explained with a large component of mafic/ultramafic lithologies. Whether these were intruded into pre-existing oceanic or continental crust cannot be resolved without additional evidence. Both the mid- and upper-crustal layers (2900 kg/m^3, 2600 kg/m^3 respectively) and upper portions of the lower crust (LC2) required large induced and remanent magnetization components to fit the observed magnetic anomalies. Although the velocities of the mid-crustal layer (6.7 to 7.1 km/s) are typically considered diagnostic of mafic oceanic crustal layer-2 (e.g. Chian et al., 2016), there is a large range of velocities (and associated densities) for serpentinized ultramafic rocks, which are a likely lithology for the Alpha Ridge. The combined thickness of the middle and upper crustal layers ranges from 5 to 10 km; which (multiplied by the calculated aerial extent) provides a volumetric estimate of (at least) 6×10^6 km^3 for the upper portion of the HAMH/HALIP. Simplistic volumetric estimates for plutonic intrusives within the lower crust are based on the assumption that the bulk density of existing crust (3000 kg/m^3) is a combination of ultramafic material (3100 kg/m^3) and lower density protolith crust. We estimate between 50% and 65% ultramafic composition, which results in volumetric estimates of between 13×10^6 km^3 and 17×10^6 km^3. We are unable to make volumetric estimates of volcanic underplating due to limitations of deep-crustal mapping. Our results indicate that the total volcanic content of the Alpha–Mendeleev ridge complex within the HAMH area to be between 19×10^6 km^3 and 23×10^6 km^3 making this one of the largest global LIPs.

Comparison of the HAMH magnetic character and pseudogravity with global LIP analogs suggests the following conclusions: (1) LIPs are generally characterized by short-wavelength, high-amplitude magnetic anomalies with a "chaotic" pattern (diagnostic of upper crustal structures) and typically have associated pseudogravity highs (diagnostic of lower crustal structures); (2) continental flood basalt provinces do not generally exhibit a large positive pseudogravity anomaly over the entire LIP area (implying a more concentrated region of mid- and lower-crustal LIP related intrusions); (3) positive pseudogravity anomaly signatures (implying deep crustal extent) are associated with the roots (i.e. plume source region) of the LIP; and (4) of the analogs we have examined in detail, the Kerguelen Plateau bears the greatest similarity to the HAMH (similar magnetic and pseudogravity character and similar overall area/volume).

We feel there are too many gaps in the understanding of Arctic geodynamics to fully constrain detailed geodynamic models, but it is important that the inferred large mass, volume and heat flow implied by LIP formation be incorporated into any viable models for the tectonic development of the High Arctic region. Further study (including, but not limited to, deep seismic refraction surveys, seismic tomography, shallow and deep crustal drilling, high-resolution bathymetry, systematic airborne potential field surveys, as well as more subsurface sample collection and geochronological characterization) is important to develop a complete understanding of the HALIP and its role in the development of the Arctic ocean basins and their vast encircling continental shelf.

Acknowledgments

We are grateful for administrative, financial, and technical support from the Extended Continental Shelf (ECS) mapping programs of the Canadian and U.S. Governments, and for extensive discussions with our colleagues at the Geological Survey of Canada, the U.S. Geological Survey, and the U.S. National Oceanic and Atmospheric Administration. Careful reviews and constructive criticism by three anonymous reviewers and by the volume editor(s) have significantly improved this paper. We would also like to thank Victoria Pease and the "Circum-Arctic Lithosphere Evolution" (CALE) working group for the opportunity to present preliminary versions of this work at various workshops and conference sessions. Earth Sciences Sector (ESS) contribution number 20160143.

References

Andersen, O.B., Knudsen, P., Berry, P.A.M., 2010. The DNSC08GRA global marine gravity field from double retracked satellite altimetry. J. Geodyn. 84, 191–199.
Andronikov, A., Mukasa, S., Mayer, L.A., Brumley, K., 2008. First recovery of submarine basalts from the Chukchi Borderland and Alpha/Mendeleev Ridge, Arctic Ocean. Eos Trans. AGU 89 (53) (Fall Meeting, abstract #V41D-2124).
Asudeh, I., Green, A.G., Forsyth, D.A., 1988. Canadian expedition to study the Alpha Ridge complex: results of the seismic refraction survey. Geophys. J. 92, 283–301.
Balkwill, H.R., 1978. Evolution of Sverdrup Basin, Arctic Canada. Am. Assoc. Pet. Geol. Bull. 62, 1004–1028.
Balkwill, H.R., 1983. Geology of Amund Ringnes, Cornwall and Haig-Thomas Islands, District of Franklin. Geol. Surv. Can. Mem. 390. http://dx.doi.org/10.4095/119499 (76 pp.).
Bamber, J.L., Layberry, R.L., Gogenini, S.P., 2001a. A new ice thickness and bed data set for the Greenland ice sheet 1: measurement, data reduction, and errors. J. Geophys. Res. 106 (D24), 33773–33780.
Bamber, J.L., Layberry, R.L., Gogenini, S.P., 2001b. A new ice thickness and bed data set for the Greenland ice sheet 2: relationship between dynamic and basal topography. J. Geophys. Res. 106 (D24), 33781–33788.
Bankey, V., et al., 2002. Digital data grids for the magnetic anomaly map of North America. US Geological Survey Open-file Report 2002-414 (http://pubs.usgs.gov/of/2002/ofr-02-414/).
Bascou, J., Delpech, G., Vauchez, A., Moine, B.N., Cottin, J.Y., Barruol, G., 2008. An integrated study of microstructural, geochemical, and seismic properties of the lithospheric mantle above the Kerguelen plume (Indian Ocean). Geochem. Geophys. Geosyst. 9 (4). http://dx.doi.org/10.1029/2007GC001879 (ISSN: 1525-2027, 26 pp., Q04036).
Blakely, R.J., 1995. Potential Theory in Gravity and Magnetic Applications. Cambridge University Press, Cambridge, UK (411 pp.).
Brumley, K.J., 2014. Geologic History of the Chukchi Borderland, Arctic Ocean. Stanford University (Thesis (Ph.D.), 251 pp.).
Brumley, K.J., Mukasa, S.B., O'Brien, T.M., Mayer, L.A., Chayes, D.N., 2013. Dredged bedrock samples from the Amerasia Basin, Arctic Ocean. AGU Fall Meeting 2013, Abstract #OS13B-1703.
Bryan, S., Ernst, R., 2008. Revised definition of large igneous provinces (LIPs). Earth Sci. Rev. 86, 175–202.
Buchan, K.L., Ernst, R., 2006. Giant dyke swarms and the reconstruction of the Canadian Arctic islands, Greenland, Svalbard and Franz Josef Land. In: Hanski, E.E.A. (Ed.), Dyke Swarms: Time Markers of Crustal Evolution. Taylor and Francis, London, pp. 27–37.
Camp, V.E., Hanan, B.B., 2008. A plume-triggered delamination origin for the Columbia River Basalt Group. Geosphere 4 (3), 480–495.
Campbell, I.H., 2005. Large igneous provinces and the mantle plume hypothesis. Elements 1, 265–270.
Chian, D., Lebedeva-Ivanova, N., 2015. Atlas of sonobuoy velocity analyses in Canada Basin. Geological Survey of Canada, Open File 7661 http://dx.doi.org/10.4095/295857 (55 pp.).
Chian, D., Jackson, H.R., Hutchinson, D.R., Shimeld, J.W., Oakey, G.N., Lebedeva-Ivanova, N., Li, Q., Saltus, R.W., Mosher, D.C., 2016. Distribution of crustal types in the Canada Basin, Arctic Ocean. In: Lane, L., Stephenson, R.A. (Eds.), Tectonophysics. Special Volume on Circum-Arctic Lithosphere Evolution 691, pp. 8–30.

Christensen, N.I., 1966. Elasticity of ultrabasic rocks. J. Geophys. Res. 71 (24), 5921–5931.
Christensen, N.I., 1976. Seismic velocities, densities, and elastic constants of basalts from DSDP Leg 35. Chapter 16 in Initial Reports of the Deep Sea Drilling Project v. 35, pp. 335–337.
Christensen, N.I., 1977. Seismic velocities of Leg 37 rocks and their geophysical implications. Chapter 12 in Initial Reports of the Deep Sea Drilling Project v. 37, pp. 389–393.
Christensen, N.I., 2004. Serpentinites, peridotites, and seismology. Int. Geol. Rev. 46, 795–816.
Christensen, N.I., Salisbury, M.H., Fountain, D.M., Carlson, R.L., 1974. Velocities of compressional and shear waves in DSDP Leg 27 basalts. Chapter 16 in Initial Reports of the Deep Sea Drilling Project. v. 27, pp. 445–449.
Christensen, N.I., Hyndman, R.D., Hull, J.M., Salisbury, M.H., 1979. Seismic velocities, electrical resistivities, densities, and porosities of basalts from DSDP Leg 46. Chapter 29 in Initial Reports of the Deep Sea Drilling Project v. 46, pp. 383–388.
Christensen, N.I., Blair, S.C., Wilkens, R.H., Salisbury, M.H., 1980a. Compressional wave velocities, densities, and porosities of basalts from Holes 417A, 417D, and 418A, DSDP Legs 51–53. Chapter 67 in Initial Reports of the Deep Sea Drilling Project v. 51–53, pp. 467–1471.
Christensen, N.I., Wilkens, R.H., Blair, S.C., Carlson, R.L., 1980b. Seismic velocities, densities, and elastic constants of volcanic breccias and basalt from DSDP Leg 59. Chapter 10 in Initial Reports of the Deep Sea Drilling Project v. 59, pp. 515–517.
Clift, P.D., Turner, J., ODP LEG 152 Scientific Party, 1995. Dynamic support by the Iceland Plume and its effect on the subsidence of the northern Atlantic margins. J. Geol. Soc. Lond. 152 (1995), 935–941.
Coffin, M.F., Eldholm, O., 1994. Large igneous provinces — crustal structure, dimensions, and external consequences. Rev. Geophys. 32 (1), 1–36.
Corfu, F., Polteau, S., Planke, S., Faleide, J.I., Svensen, H., Zayoncheck, A., Stolbov, N., 2013. U–Pb geochronology of Cretaceous magmatism on Svalbard and Franz Josef Land, Barents Sea Large Igneous Province. Geol. Mag. 150 (6), 1127–1135.
Courtier, A.M., Hart, D.J., Christensen, N.I., 2004. Seismic properties of Leg 195 serpentinites and their geophysical implications. In: Shinohara, M., Salisbury, M.H., Richter, C. (Eds.), Proc. ODP, Sci. Results v. 195, pp. 1–12.
Døssing, A., Jackson, H.R., Matzka, J., Einarsson, I., Rasmussen, T.M., Olesen, A.V., Brozena, J.M., 2013. On the origin of the Amerasian basin and the High Arctic Large Igneous Province — results of new aeromagnetic data. Earth Planet. Sci. Lett. 363, 219–230.
Dove, D., Coakley, B., Hopper, J., Kristoffersen, Y., HLY0503 Geophysics Team, 2010. Bathymetry, controlled source seismic and gravity observations of the Mendeleev Ridge: implications for ridge structure, origin, and regional tectonics. Geophys. J. Int. 183, 481–502.
Embry, A.F., 1989. Correlation of Upper Paleozoic and Mesozoic sequences between Svalbard, Canadian Arctic Archipelago, and northern Alaska. In: Colinson, J.D. (Ed.), Correlation in Hydrocarbon Exploration. Graham and Trotman, London, pp. 89–99.
Embry, A.F., 1991. Mesozoic history of the Arctic islands. In: Trettin, H.P. (Ed.), Geology of the Innuitian Orogen and Arctic Platform of Canada and Greenland. Geological Survey of Canada, Geology of Canada 3, pp. 371–433.
Embry, A.F., Osadetz, K.G., 1988. Stratigraphy and tectonic significance of Cretaceous volcanism in the Queen Elizabeth Islands, Canadian Arctic Archipelago. Can. J. Earth Sci. 25, 1209–1219.
Ernst, R., Bleeker, W., 2010. Large igneous provinces (LIPS), giant dyke swarms, and mantle plumes: significance for breakup events within Canada and adjacent regions from 2.5 Ga to the present. Can. J. Earth Sci. 47 (5), 695–739.
Ernst, R., Buchan, K., 2001. Large mafic magmatic events through time and links to mantle plume heads. Geological Society of America Special Paper 352, Mantle Plumes Their Identification through Time, pp. 483–575.
Escher, J.C., and Pulvertaft, T.C.R., 1995. Geological map of Greenland, 1:250000. Copenhagen: Geological Survey of Greenland.
Estrada, S., 2015. Geochemical and Sr–Nd isotope variation within Cretaceous continental flood-basalt suites of the Canadian High Arctic, with a focus on the Hassel Formation basalts of northeast Ellesmere Island. Int. J. Earth Sci. 104, 1981–2005. http://dx.doi.org/10.1007/s00531-014-1066-x.
Estrada, S., Henjes-Kunst, F., 2004. Volcanism in the Canadian High Arctic related to the opening of the Arctic Ocean. Z. Dtsch. Geol. Ges. Geowiss. (Ger. J. Geosci.) 154, 579–603.
Estrada, S., Henjes-Kunst, F., 2013. 40Ar–39Ar and U–Pb dating of Cretaceous continental rift-related magmatism on the northeast Canadian Arctic margin. Z. Dtsch. Ges. Geowiss. (Ger. J. Geosci.) 164, 107–130. http://dx.doi.org/10.1127/1860-1804/2013/0005.
Estrada, S., Damaske, D., Henjes-Kunst, F., Schreckenberger, B., Oakey, G.N., Piepjohn, K., Eckelmann, K., Linnemann, U., 2016. Multistage Cretaceous magmatism in the northern coastal region of Ellesmere Island and its relation to the formation of Alpha Ridge — evidence from aeromagnetic, geochemical and geochronological data. Proceedings From the International Conference on Arctic Margins VII; Trondheim 96 (2), p. 32. http://dx.doi.org/10.17850/njg96-2-03.
Evenchick, C.A., Davis, W.J., Bédard, J.H., Hayward, N., Friedman, R.M., 2015. Evidence for protracted High Arctic large igneous province magmatism in the central Sverdrup Basin from stratigraphy, geochronology, and paleodepths of saucer-shaped sills. Geol. Soc. Am. Bull. http://dx.doi.org/10.1130/B31190.1.
Forsyth, D.A., Mair, J.A., 1984. Crustal structure of the Lomonosov Ridge and the Fram and Makarov basins near the north pole. J. Geophys. Res. 89 (B1), 473–481.
Forsyth, D.A., Asudeh, I., Green, A.G., Jackson, H.R., 1986a. Crustal structure of the Northern Alpha Ridge beneath the Arctic Ocean. Nature 322, 349–352.
Forsyth, D.A., Morel-l'Huissier, P., Asudeh, I., Green, A.G., 1986b. Alpha Ridge and Iceland — products of the same plume? J. Geodyn. 6, 197–214.
Foulger, G.R., 1988. Hengill Triple Junction, SW Iceland, part 1: tectonic structure and the spatial and temporal distribution of local earthquakes. J. Geophys. Res. 93-Bll (13), 493–13,506.
Frey, F.A., Coffin, M.F., Wallace, P.J., Weis, D., Zhao, X., Wise Jr., S.W., Wahnert, V., Teagle, D.A.H., Saccocia, P.J., Reusch, D.N., Pringle, M.S., Nicolaysen, K.E., Neal, C.R., Muler, R.D., Moore, C.L., Mahoney, J.J., Keszthelyi, L., Inokuchi, H., Duncan, R.A., Delius, H., Damuth, J.E., Damasceno, D., Coxall, H.K., Borre, M.K., Boehm, F., Barling, J., Arndt, N.T., Antretter, M., 2000. Origin and evolution of a submarine large igneous province: the Kerguelen Plateau and Broken Ridge, southern Indian Ocean. Earth Planet. Sci. Lett. 176, 73–89.
Funck, T., Jackson, H.R., Shimeld, J., 2011. The crustal structure of the Alpha Ridge at the transition to the Canadian Polar Margin — results from a seismic refraction experiment. J. Geophys. Res. B Solid Earth 116 (B12101). http://dx.doi.org/10.1029/2011JB008411 (26 pp.).
Gaina, C., Werner, S., Saltus, R., Maus, S., the CAMP-GM Group, 2011. Circum-Arctic Mapping Project — new magnetic and gravity anomaly maps of the Arctic. In: Spencer, A.M., et al. (Eds.), Arctic Petroleum Geology. Geological Society of London Memoir 35, pp. 39–48.
Gaina, C., Medvedev, S., Torsvik, T.H., Koulakov, I., Werner, S.C., 2014. 4D Arctic — a glimpse into the structure and evolution of the Arctic in the light of new geophysical maps, plate tectonics and tomographic models. Surv. Geophys. 35, 1095–1122. http://dx.doi.org/10.10007/s10712–013-9254-y.
Grantz, A., Scott, R.A., Drachev, S.S., Moore, T.E., 2009. Map showing the sedimentary successions of the Arctic region that may be prospective for hydrocarbons. American Association of Petroleum Geologists, Tulsa, OK, GIS-UDRIL Open-File Spatial Library.
Grantz, A., Hart, P., Childers, V., 2011. Geology and tectonic development of the Amerasia and Canada Basins, Arctic Ocean: Arctic petroleum geology. In: Spencer, A.M., Embry, A.F., Gautier, D.L., Stoupakova, A.V., Sorensen, K. (Eds.), Geological Society of London Memoir 35, pp. 771–799.
Hales, T.C., Abt, D.L., Humphreys, E.D., Roering, J.J., 2005. A lithospheric instability origin for Columbia River flood basalts and Wallowa Mountains uplift in northeast Oregon. Nature 438 (8), 842–845. http://dx.doi.org/10.1038/nature04313.
Harrison, J.C., St-Onge, M.R., Petrov, O.V., Strelnikov, S.I., Lopatin, B.G., Wilson, F.H., Tella, S., Paul, D., Lynds, T., Shokalsky, S.P., Hults, C.K., Bergman, S., Jepsen, H.F., Solli, A., 2011. Geological map of the Arctic/Carte géologique de l'Arctique. Geological Survey of Canada. "A" Series Map 2159A, 9 Sheets; 1 DVD http://dx.doi.org/10.4095/287868.
Hegewald, A., Jokat, W., 2013. Relative sea level variations in the Chukchi region – Arctic Ocean – since the late Eocene. Geophys. Res. Lett. 40, 803–807. http://dx.doi.org/10.1002/GRL.50182.
Houseknecht, D.W., Bird, K.J., 2011. Geology and petroleum potential of the rifted margins of the Canada Basin. In: Spencer, A.M., Embry, A.F., Gautier, D.L., Stoupakova, A.V., Sørensen, K. (Eds.), Arctic Petroleum Geology. Geological Society, London, Memoir 35, pp. 509–526.
Jackson, H.R., Mudie, P.J., Blasco, S.M., 1985. Initial geological report on CESAR — the Canadian Expedition to Study the Alpha Ridge. Geological Survey of Canada,. Paper 84–22 (177 pp.).
Jakobsson, M., Mayer, L., Coakley, B., Dowdswell, J., Forbes, S., et al., 2012. The International Bathymetric Chart of the Arctic Ocean (IBCAO) version 3.0. Geophys. Res. Lett. 39, L12609. http://dx.doi.org/10.1029/2012GRL052219 (6 pp.).
Jokat, W., Ickrath, M., O'Connor, 2013. Seismic transect across the Lomonsov and Mendeleev Ridges — constraints on the geological evolution of the Amerasia Basin, Arctic Ocean. Geophys. Res. Lett. 40, 5047–5051.
Kenyon, S.C., Forsberg, R., Coakley, B., 2008. New gravity field for the Arctic. EOS Trans. Am. Geophys. Union 89, 289–290.
King, E.R., Zietz, I., Alldredge, L., 1964. Genesis of the Arctic Ocean Basin. Science 144, 1551–1557.
King, E.R., Zietz, I., Alldredge, L., 1966. Magnetic data on the structure of the Central Arctic region. GSA Bull. 77 (619-464).
Kingsberry, C.G., Ernst, R.E., Cousens, B., Williamson, M.-C., 2014. Geochemical insights on the Early Cretaceous High Arctic LIP. Geological Society of America Annual Meeting, Paper No. 260–9 (https://gsa.confex.com/gsa/2014AM/finalprogram/abstract_243832.htm).
Lawver, L.A., Mueller, R.D., 1994. Iceland hotspot track. Geology 22 (4), 311–314.
Lawver, L.A., Scotese, C.R., 1990. A review of tectonic models for the evolution of the Canada basin. In: Grantz, A., Johnson, G.L., Sweeney, J.F. (Eds.), The Arctic Ocean Region. Boulder, Colorado, Geological Society of America, the Geology of North America L, pp. 593–618.
Lebedeva-Ivanova, N.N., Zamansky, Y.Y., Langinen, A.E., Sorokin, M.Y., 2006. Seismic profiling across the Mendeleev Ridge at 82°N: evidence of continental crust. Geophys. J. Int. 165, 527–544.
Lobkovsky, L., 2015. Model of the Arctic evolution since the Cretaceous to present, based on upper mantle convection linked with Pacific lithosphere subduction. EGU General Assembly 2015 v. 17, pp. EGU2015–EGU2426.
Ludwig, W.J., Nafe, J.E., Drake, C.L., 1970. In: Maxwell, A.E. (Ed.), Seismic Refraction. In the Sea, Vol. 4, New Concepts of Sea Floor Evolution, Part I. Wiley Interscience, Hoboken, N.J., pp. 53–84.
Lundin, E.R., Doré, A.G., 2005. NE Atlantic break-up: a re-examination of the Iceland mantle plume model and the Atlantic–Arctic linkage. In: Doré, A.G., Vining, B.A. (Eds.), Petroleum Geology: North-West Europe and Global Perspectives—Proceedings of the 6th Petroleum Geology Conference© Petroleum Geology Conferences Ltd.Geological Society, London, pp. 739–754.
Maher Jr., H.D., 2001. Manifestations of the Cretaceous High Arctic Large Igneous Province in Svalbard. J. Geol. 109 (1), 91–104.
Maus, S., et al., 2009. EMAG2: a 2-arc min resolution earth magnetic anomaly grid complied from satellite, airborne, and marine magnetic measurements. Geochem. Geophys. Geosyst. 10 (8). http://dx.doi.org/10.1029/2009GC002471.
Meyer, R., Wijk, J., Gernigon, L., 2007. North Atlantic Igneous Province — a review of models for its formation. GSA Special Paper 430, pp. 525–552.

Midtkandal, I., Nystuen, J.P., 2009. Depositional architecture of a low-gradient ramp shelf in an epicontinental sea — the lower Cretaceous of Svalbard. Basin Res. 21, 655–675.
Miller, E.L., Gehrels, G.E., Pease, V., Sokolov, S., 2010. Stratigraphy and U–Pb detrital zircon geochronology of Wrangel Island, Russia — implications for Arctic paleogeography. AAPG Bull. 94 (5), 665–692.
Morozov, A., Petrov, O., Kremenetskiy, A., Kashubin, S., Rekant, P., Gusev, E., Shokalsky, S., Shevchenko, S., Sergeev, S., Artyuchkov, E., 2013a. Geological and geochemical criteria for the continental nature of the Mendeleev Rise (the Arctic Ocean) from the data of drilling and dredging of seabed rock material. EGU General Assembly, April 2013, pp. EGU2013–EG11061.
Morozov, A.F., Petrov, O.V., Shokalsky, S.P., Kashubin, S.N., Kremenetsky, A.A., Shkatov, M.Y., Kaminsky, V.D., Gusev, E.A., Grikurov, G.E., Rekant, P.V., Shevchenko, S.S., Sergeev, S.A., Shatov, V.V., 2013b. New geological data are confirming continental origin of the Central Arctic Rises. Regionalnaya Geologia I Metallogenia (Regional geology and metallogeny) No. 53pp. 34–55 (in Russian).
Mosher, D.C., Shimeld, J.D., Hutchinson, D.R., 2009. 2009 Canada Basin seismic reflection and refraction survey, western Arctic Ocean. CCGS Louis S. St-Laurent Expedition Report, Geological Survey of Canada Open File 6343 (266 pp.).
Mukasa, S., Adronikov, A., Mayer, L., Brumley, K.J., 2009. Geochemistry and geochronology of the first intraplate lavas recovered from the Arctic Ocean. GSA Annual Meeting 2009, Paper No. 138–11 (https://gsa.confex.com/gsa/2009AM/finalprogram/abstract_165321.htm).
Mukasa, S.B., Mayer, L.A., Aviado, K., Bryce, J., Adronikov, A., Brumley, K., Blichert-Toft, J., Petrov, O., Shokalsky, S., 2015. Alpha–Mendeleev Ridge and Chukchi Borderland Ar 40/39 geochronology and geochemistry — character of the first submarine intraplate lavas recovered from the Arctic Ocean. EGU General Assembly 2015 v. 17 (EGU2015–8291-2).
Müller, R.D., Royer, J.-Y., Lawver, L.A., 1993. Revised plate motions relative to the hotspots from combined Atlantic and Indian Ocean hotspot tracks. Geology 21, 275–278.
Nady, D., 1966. The gravitational attraction of a right rectangular prism. Geophysics 31 (2), 362–371.
Nicolaysen, K., Frey, F.A., Hodges, K.V., Weis, D., Giret, A., 2000. 40Ar/39Ar geochronology of flood basalts from the Kerguelen Archipelago, southern Indian Ocean: implications for Cenozoic eruption rates of the Kerguelen plume, Earth Planet. Sci. Lett. 174, 313–328. http://dx.doi.org/10.1016/S0012-821X(99) 00271-X.
Oakey, G.N., 2005. Cenozoic Evolution and Lithosphere Dynamics of the Baffin Bay — Nares Strait Region of Arctic Canada and Greenland (PhD Thesis) Vrije Universiteit, The Netherlands (233 pp., ISBN 0-09739355-0-2).
Oakey, G.N., Stephenson, R.A., 2008. Crustal structure of the Innuitian region of Arctic Canada and Greenland from gravity modelling: implications for the Palaeogene Eurekan Orogen. Geophys. J. Int. 173 (3), 1039–1063.
Osadetz, K.G., Moore, P.R., 1988. Basic volcanics in the Hassel Formation (Mid-Cretaceous) and associated intrusives, Ellesmere Island, District of Franklin, Northwest Territories. Geological Survey of Canada, Paper 87–21 (19 pp.).
Ostenso, N.A., 1962. Geophysical investigations of the Arctic Ocean Basin. University of Wisconsin, Geophysical and Polar Research Center Research Report Series 62-4 (124 pp.).
Ostenso, N.A., Wold, R.J., 1971. Aeromagnetic survey of the Arctic Ocean — techniques and interpretations. Mar. Geophys. Res. 1, 178–219.
Pavlis, N.K., Holmes, S.A., Kenyon, S.C., Factor, J.K., 2008. An earth gravitational model to degree 2160. Geophys. Res. (Abstract 10, EGU2008-A-01891, 1607-7962/gra/EGU2008-A- 01891, EGU General Assembly).
Petrov, O., Morozov, A., Shokalsky, S., Sobolev, N., Kashubin, S., Shevchenko, S., Sergeev, S., Belyatsky, B., Shatov, V., Petrov, E., 2015. Igneous rocks of the Arctic ocean deep sea ridges — new data on petrology, geochemistry and geochronology. EGU General Assembly 2015 v. 17, pp. EGU2015–EGU2373.
Piskarev, A.L., 2004. The basement structure of the Eurasian Basin and central ridges in the Arctic Ocean. Geotectonics 38, 443–458.
Reichow, M.K., Pringle, M.S., Al'Mukhamedo, A.I., Allen, M.B., Andreichev, V.L., Buslov, M.M., Davies, C.E., Fedoseev, G.S., Fitton, J.G., Inger, S., Medvedev, A.Y., Mitchell, C., Puchkov, V.N., Safonov, I.Y., Scott, R.A., Saunders, A.D., 2009. The timing and extent of the eruption of the Siberian Traps large igneous province: implications for the end-Permian environmental crisis. Earth Planet. Sci. Lett. 277, 9–20 (10.1016/j.epsl.2008.09.30).
Reidel, S.P., Camp, V.E., Tolan, T.L., Kauffman, J.D., Garwood, D.L., 2013. Tectonic evolution of the Columbia River flood basalt province. In: Reidel, S.P., Camp, V.E., Ross, M.E., Wolff, J.A., Martin, B.S., Tolan, T.L., Wells, R.E. (Eds.), The Columbia River Flood Basalt Province: Geological Society of America Special Paper 497, pp. 293–324 http://dx.doi.org/10.1130/2013.2497(12).
Ricketts, B., Osadetz, K.G., Embry, A.F., 1985. Volcanic style in the Strand Fiord Formation (Upper Cretaceous), Axel Heiberg Island, Canadian Arctic Archipelago. Polar Res. 3, 107–122.
Salisbury, M.H., Christensen, N.I., 1976. Sonic velocities and densities of basalts from the Nazca Plate, DSDP Leg 34. Chapter 45 in Initial Reports of the Deep Sea Drilling Project v. 34, pp. 543–546.
Saltus, R.W., Oakey, G.N., 2015. Magnetic subdomains of the High Arctic Magnetic High — speculations and implications for understanding of the High Arctic Large Igneous Province and related tectonics. AGU Fall Meeting 2015, Abstract T51B-2877 (Poster).
Saltus, R.W., Miller, E.L., Gaina, C., Brown, P.J., 2011. Regional magnetic domains of the Circum-Arctic — a framework for geodynamic interpretation. In: Spencer, A.M., et al. (Eds.), Arctic Petroleum Geology. Geological Society of London Memoir 35, pp. 49–60.
Schreiber, E., Fox, P.J., 1977. Density and P-wave velocity of rocks from the FAMOUS region and their implication on the structure of the oceanic crust. Geol. Soc. Am. Bull. 88, 60–608.
Shephard, G.E., Mueller, R.D., Seton, M., 2013. The tectonic evolution of the Arctic since Pangea breakup — integrating constraints from surface geology and geophysics with mantle structure. Earth Sci. Rev. 124, 148–183.
Sleep, N.H., 1990. Hotspots and mantle plumes: some phenomenology. J. Geophys. Res. 95, 6715–6736.
Sleep, N.H., 1992. Hotspot volcanism and mantle plumes. Annu. Rev. Earth Planet. Sci. 20, 19–43.
Sobolev, S.V., Sobolev, A.V., Kuzmin, D.V., Krivolutskaya, N.A., Petrunin, A.G., Arndt, N.T., Radko, V.A., Vasiliev, Y.R., 2011. Linking mantle plumes, large igneous provinces and environmental catastrophes. Nature 477, 312–316. http://dx.doi.org/10.1038/nature10385.
Tarduno, J.A., 1998. The High Arctic Large Igneous Province. Abstract, Int. Conf. Arctic Margins (ICAM III), Celle, Germany, Fed. Inst. Geosci. Nat. Res.
Taylor, P.T., Kovacs, L.C., Vogt, P.R., Johnson, G.L., 1981. Detailed aeromagnetic investigation of the Arctic Basin, 2. J. Geophys. Res. 86 (B7), 6323–6333.
Taylor, A., Judge, A., Allen, V., 1986. Terrestrial heat flow from Project CESAR, Alpha Ridge, Arctic Ocean. J. Geodyn. 6, 137–176.
Tegner, C., Storey, M., Holm, P.M., Thorarinsson, S.B., Zhao, X., Lo, C.H., Knudsen, M.F., 2011. Magmatism and Eurekan deformation in the High Arctic Large Igneous Province — 40Ar–39Ar age of Kap Washington Group volcanics, North Greenland. Earth Planet. Sci. Lett. 311, 195–196.
Treshnikov, A.F., Balakshin, L.L., Belov, N.A., Demenitskaya, R.M., Dibner, V.D., Karasik, A.M., Shpeiker, A.O., Shurgayeva, N.D., 1966. A geographic nomenclature for the chief topographic features, the bottom of the Arctic Basin. Problems of the Arctic and Antarctic 27, pp. 1–25.
Torsvik, T.H., Smethurst, M.A., Burke, K., Steinberger, B., 2006. Large igneous provinces generated from the margins of the large low-velocity provinces in the deep mantle. Geophys. J. Int. 167, 1447–1460.
Trettin, H.P., Parrish, R., 1987. Late Cretaceous bimodal magmatism, northern Ellesmere Island: isotopic age and origin. Can. J. Earth Sci. 24, 257–265.
Van Wagoner, N.A., Williamson, M.-C., Robinson, P.T., Gibson, I.L., 1986. First samples of acoustic basement recovered from the Alpha Ridge, Arctic Ocean: new constraints for the origin of the ridge. J. Geodyn. 6, 177–196.
Verhoef, J., Roest, W., Macnab, R., Arkani-Hamed, J., Members of the Project Team (Kovacs, S., Levesque, S., Morris, P., Oakey, G., Srivastava, S., Stark, A., Usow, K., and Vardy, D.), 1996. A compilation of magnetic observations from the Arctic and North Atlantic Oceans and adjacent land areas (CD-ROM data release). Geological Survey of Canada, Open File 3125a.
Villeneuve, M., Williamson, M.-C., 2006. 40Ar–39Ar dating of mafic magmatism from the Sverdrup Basin Magmatic Province. In: Scott, R.A., Thurston, D.K. (Eds.), Proceedings of the Fourth International Conference on Arctic Margins, OCS Study, MMS 2006–003. U.S. Department of the Interior, pp. 206–215.
Vogt, P.R., Ostenso, N.A., 1980. Magnetic and gravity profiles across the Alpha Cordillera and their relationship to Arctic sea-floor spreading. J. Geophys. Res. 75, 4925–4938.
Vogt, P., Taylor, P., Kovacs, L., et al., 1979. Detailed aeromagnetic investigation of the Arctic Basin. J. Geophys. Res. 84, 1071–1089.
Vogt, P.R., Jung, W., Jakobsson, M., Mayer, L., Williamson, M., 2006. The Alpha–Mendeleev Magmatic Province, Arctic Ocean — a new synthesis. Eos 87, 36.
Walker, J.D., and Geissman, J.W., compilers, 2009, Geologic Time Scale: Geological Society of America, http://dx.doi.org/10.1130/2009.CTS004R2C. ©2009 The Geological Society of America.
Weber, J.R., 1986. The Alpha Ridge: gravity, seismic, and magnetic evidence for a homogeneous, mafic crust. J. Geodyn. 6, 117–136.
Weber, J.R., 1990. The structures of the Alpha Ridge, Arctic Ocean and Iceland–Faeroe Ridge, North Atlantic: comparisons and implications for the evolution of the Canada Basin. Mar. Geol. 93, 43–68.
Weigand, P.W., Testa, S.M., 1982. Petrology and geochemistry of Mesozoic dolerites from the Hinlopenstretet area, Svalbard. Polar Res. 1, 35–52.
White, R.S., 1989. Initiation of the Iceland plume and opening of the North Atlantic. In: Tankard, A.J., Balkwill, H.R. (Eds.), Extensional Tectonics and Stratigraphy of the North Atlantic Margins. AAPG Mem. 46, pp. 149–154.
Whitechurch, H., Montigny, R., Sevigny, J., Storey, M., Salters, V., 1992. K–Ar and 40Ar–39Ar ages of central Kerguelen Plateau basalts. In: Wise, W.S., Schlich, R., et al. (Eds.), Proc. Ocean Drill. Prog., Scientific Results 120. Ocean Drill. Prog., College Station, TX, 1992, pp. 71–77.
Worsley, D., 1986. The Geological History of Svalbard — Evolution of an Arctic Archipelago. Den Norske Stats Oljeselskap, Stavanger, Norway (121 pp.).
Zwally, H.J., et al., 2002. ICESat's laser measurement of polar ice, atmosphere, ocean and land. J. Geodyn. 34 (3–4), 405–445.